



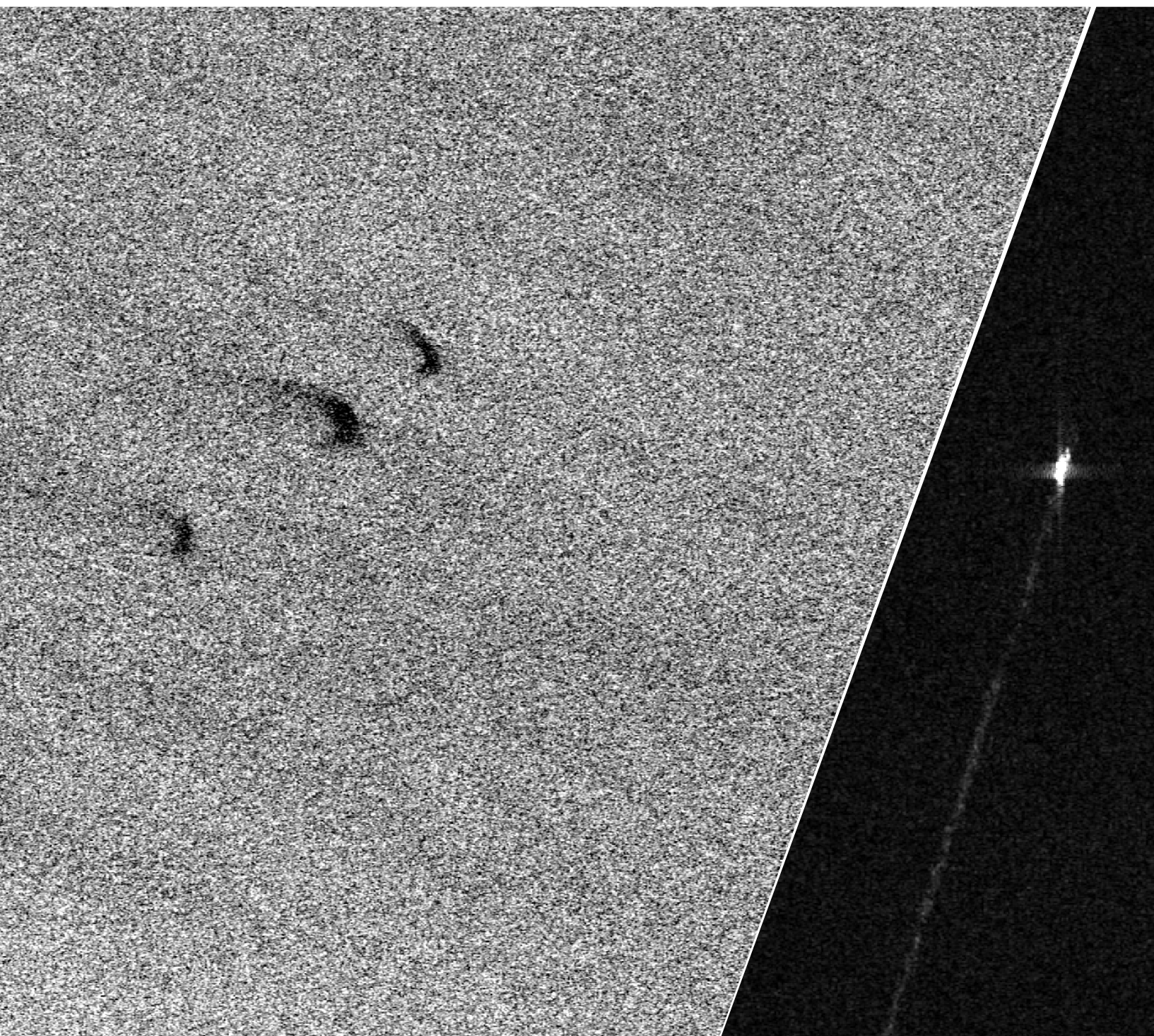
UiT The Arctic University of Norway

Faculty of Science and Technology
Department of Physics and Technology

Natural occurring oil seepages as a consequence of bottom trawling?

Sander Hindenes

FYS-3931 Master's thesis in Space Physics 30 SP
June 2023



This thesis document was typeset using the *UiT Thesis L^AT_EX Template*.
© 2023 – <http://github.com/egraff/uit-thesis>

The front page show excerpts from two Sentinel-1 Synthetic Aperture Radar images. The left image shows three oil slicks observed by Sentinel-1B on 2020.05.06. The right image shows a vessel and its wake observed by Sentinel-1A on 2020.05.07

Abstract

Bottom trawling is used to capture fish species that live in the seabed. The damage on the seabed trawling causes has been discussed for many years. This thesis aims to investigate whether bottom trawling for sand eels can be a cause for some of the detected oil seepages in the North Sea. We investigated this using manual delineation of oil seepages in Synthetic Aperture Radar (SAR) satellite images to create statistics of when and where oil observations have been made; in total three areas were investigated. The SAR observations have been coupled together with wind speed data and trawling tracks. In 2020, an average of 76 % of the oil seepage observations were made during the sand eel trawling season. In 2021 there was a sudden drop in trawling activity with half the total number of trawling tracks. The sudden drop in trawling activity for 2021 greatly reduced the number of observations of oil slicks, but one of the three investigated areas showed a similar number of observations inside the trawling season. Using the trawling track information it was observed that areas with higher amounts of trawling activity have a higher number of seepage observations. For three of the datasets a p-value below 0.05 was confirmed, based on a null hypothesis of neither favouring observation of an oil slick during or outside of sand eel trawling season. Notably the statistics of observations implies a significant correlation between trawling activity and oil slick observations, which warrants further study or observation.

Acknowledgements

First and foremost, I would like to thank my supervisor Malin Johansson for introducing me to this topic. Your patience, discussion and guidance has been incredibly helpful these short months. This project has been a fulfilling end to my time at UiT.

I would like to thank my brother Lars for taking time out of his day to proofread this thesis.

I would like to thank Ingeborg for helpful discussions, input and support.

I would like to thank my parents Tove and Jørn for supporting me through my education and always believing in me.

I would like to thank Rune Mattingsdal from The Norwegian Petroleum Directorate for sharing insight about trawling activity and the seasonal sand eel fishing.

I would like to thank The Norwegian Directorate of Fisheries for supplying the trawling track data used in this thesis.

I would like to thank The European Space Agency for providing the Sentinel-1 SAR data. The thesis contains Sentinel-1 Copernicus data (2020,2021).

Contents

Abstract	iii
Acknowledgements	v
List of Figures	ix
List of Tables	xiii
1 Introduction	1
2 Background	3
2.1 Radar	3
2.2 Electromagnetic Waves	4
2.2.1 Frequency bands and corresponding applications . .	4
2.2.2 Polarization of electromagnetic waves	4
2.2.3 Signal and noise in radars	5
2.3 Synthetic Aperture Radar (SAR)	6
2.3.1 SAR incidence angle	7
2.3.2 Pre-processing and calibration	9
3 SAR Imaging for marine surface oil slick detection	13
3.1 Advantage of using SAR for oil slick monitoring	14
3.2 Challenges or disadvantages	14
3.3 Theory for differentiating open sea and oil slick	16
3.3.1 Scattering mechanisms	16
3.3.2 Relative permittivity (Dielectric constant)	17
3.3.3 Wind	17
4 Study areas and data sets	19
4.1 Sand eel fishing - bottom trawling	20
4.2 Sentinel-1	21
4.2.1 Acquisition modes of Sentinel-1	22
4.3 Wind data	22
4.4 Fishing boat tracks	23

5 Method	25
5.1 SAR data	25
5.1.1 Subsetting	25
5.1.2 Geocoding	26
5.1.3 Delineation	26
5.2 Wind data	26
5.2.1 Ekofisk	26
5.2.2 SAR wind	27
6 Results and discussion	29
6.1 Number of observations and amount of trawling activity	29
6.2 Observed oil slicks, time of year and wind speed	31
6.3 Reoccurring oil slick locations	33
6.4 Distance to closest trawling track	34
6.5 Combined observations	35
7 Conclusion and future work	39
7.1 Future work	40
A Appendix	41
A.1 Additional figures	41
A.1.1 Observations	41
A.1.2 Heatmaps	47
A.1.3 Proximity plots	49
Bibliography	53

List of Figures

2.1	Illustration of a vertically polarized wave along the y-z plane, and a horizontally polarized wave along the x-z plane.	5
2.2	As the satellite moves in the azimuth direction it makes multiple observations along the path. The first observation has the vessel at the edge of the observation. The middle observation has the vessel at the center, and finally the last observation is done just as it leaves the view of the satellite. If the vessel is standing still, the length of the synthetic antenna is the distance from the first to the last observation.	6
2.3	Illustration of how the incidence angle impacts the return signal. For low incidence angle θ_2 the backscattered signal has a higher return. In far range for incidence angle θ_1 the signal is lower and therefore darker.	8
2.4	Sentinel-1A image from 2020.05.24 that shows the phenomena of a higher backscatter power in near range (left side of image), while less backscatter power in far range (right side of image). The image contains open water.	8
2.5	A Sentinel-1A image from 2020-04-18 calibrated to Sigma zero. The bright spot is a vessel with a wake. The brighter tail behind is the turbulent wake as the ship moves through a low wind ocean.	10
2.6	A Sentinel-1A image from 2020-04-18 calibrated to Sigma zero with a 5x5 multi-looked window. The image is the same as seen in Figure 2.5.	11
3.1	Example image of surface slicks observed in a Sentinel-1A image from the 7th of May 2020.	13
3.2	Image taken by Sentinel-1A 2020.06.10. The dark section in the north is an area of low wind speeds. The image has been calibrated to sigma nought, and multi-looked with a 3x3 window.	15

3.3	In the top illustration the power of the backscattered signal is illustrated as equally sized arrows. The arrows show how it would be difficult to differentiate oil and the areas of calm ocean due to low wind. While the bottom shows an increase in backscatter of areas of high wind and rough ocean. The oil dampens the ocean waves and creates an area of lower power backscatter. (The arrows only illustrate how the surface of the ocean impacts backscattered power, and should not be used as a comparison between scenarios.)	16
4.1	Map showing Area 1 in red, Area 2 in orange, and Area 3 in green. The dotted line is the EEZ of Norway. The blocks are used by NPD as a geographical unit for division in the petroleum sector on the Norwegian continental shelf.	20
4.2	Illustration of the geometry of the different acquisition modes [5]. Copyrights: European Space Agency - ESA	22
4.3	Wind speed values from Ekofisk to illustrate the range of wind speeds for each month.	23
4.4	Illustration of all 29000 trawling tracks from 2020 to 2021 in red. The density of trawlers varies, but Area 1, Area 2, and Area 3 have areas of increased trawling activity.	24
6.1	Graph of the number of trawlers per day. Outside the Sand eel season there is a big drop in number of tracks per day. When comparing the Sand eel season in 2020 and 2021 there seems to be decrease in activity in 2021.	30
6.2	Area 1 images with or without observation in 2020 with wind data from Ekofisk.	32
6.3	Area 1 images with or without observation in 2020 with wind data from SARwind.	32
6.4	All polygons from Area 1 in 2020. Illustrated as a heatmap, and shows any overlapping polygons as a color indicated by the colorbar.	33
6.5	Polygons for each slick in 2020 in area 1. The color illustrates the distance away from the nearest trawling track in meters. A yellow polygon has a trawling track from the same day that has been very close, while a dark blue / purple polygon has a trawling track that is further away.	34
A.1	Area 2 observation in 2020 with wind data from Ekofisk . .	42
A.2	Area 2 observation in 2020 with wind data from SARwind . .	42
A.3	Area 3 observation in 2020 with wind data from Ekofisk . .	43
A.4	Area 3 observation in 2020 with wind data from SARwind . .	43
A.5	Area 1 observation in 2021 with wind data from Ekofisk . .	44

A.6 Area 1 observation in 2021 with wind data from SARwind	44
A.7 Area 2 observation in 2021 with wind data from Ekofisk	45
A.8 Area 2 observation in 2021 with wind data from SARwind	45
A.9 Area 3 observation in 2021 with wind data from Ekofisk	46
A.10 Area 3 observation in 2021 with wind data from SARwind	46
A.11 Heatmap of overlapping observations for area 2 in 2020	47
A.12 Heatmap of overlapping observations for area 3 in 2020	47
A.13 Heatmap of overlapping observations for area 1 in 2021	48
A.14 Heatmap of overlapping observations for area 2 in 2021	48
A.15 Heatmap of overlapping observations for area 3 in 2021	49
A.16 Plot of all polygons colored after the distance to the closest trawler. Observations from 2020 in area 2.	49
A.17 Plot of all polygons colored after the distance to the closest trawler. Observations from 2020 in area 3.	50
A.18 Plot of all polygons colored after the distance to the closest trawler. Observations from 2021 in area 1.	50
A.19 Plot of all polygons colored after the distance to the closest trawler. Observations from 2021 in area 2.	51
A.20 Plot of all polygons colored after the distance to the closest trawler. Observations from 2021 in area 3.	51

List of Tables

2.1	Overview of the different bands, showing their associated frequency, wavelength, and the application typical for that band [4].	4
3.1	Boon Agreement Oil Appearance Code labels that show the layer thickness and volume related to each specific code. Commonly used for optical oil classification.	15
4.1	Overview of the data used for this thesis, date, the mode and which satellite acquired the data.	21
4.2	List of characteristics of Sentinel-1 IW acquisition mode. . .	21
6.1	Overview of the number of images and the number of observations for each area in 2020 and 2021.	30
6.2	Total number of trawling tracks inside the season window in Figure 6.1.	31
6.3	Overview of the total number of observations for each area in 2020 and 2021. The percentage shows the ratio of images with observation inside the sand eel trawling season to the total number of observations.	37

/ 1

Introduction

Earth observation is a global industry, and the use of Synthetic Aperture Radar (SAR) has emerged as an important tool for monitoring the Earth. SAR is a type of Radio Detection and Ranging (radar) instrument which is used by national governments and corporations. SAR enables collection of a wide range of information for studies about land, including the topics such as crops, forests, cities and minerals [16; 18]. Another large field of studies is ocean monitoring, which include collecting information about different types of vessels, oil platforms, ice prevalence and movement, oil spills, to name a few examples [3]. It allows for monitoring of the ocean surface for early detection of oil spill disasters, and is a tool that can assist in cleanup operations by identifying changes in spread and location and identify area of increased volume.

SAR has the ability to detect areas of marine surface oil slicks, though there are different types of oil that can occur on the ocean surface, natural seepages are a phenomena that occurs on the seabed when pockets of natural gasses and mineral oils float to the ocean surface, fishing boats can release fish oil during fishing operations, and of course oil platforms and vessels can have accidents and for some reason start leaking oil into the ocean [3]. Oil detection is possible due to the dampening of the ocean surface waves, making the ocean surrounding an oil spill rough compared to the oil slick in the SAR image, hence showing up as a dark spot. This contrast between areas of oil and clean sea allows us to identify surface oil by looking at SAR images. Other phenomena that can results in damping of the surface waves are low wind speeds, which creates less waves on the ocean surface.

Bottom trawling is a controversial topic regarding its impact on the seabed through the scraping and the damage it can cause [13]. The scraping of the sediments on the sea bed could cause oil to rise up to the ocean surface. In the North Sea bottom trawling for sand eels is a seasonal type of fishing and occurs from the middle of April until late June in the Norwegian Exclusive Economic Zone [11]. This period of trawling is the basis of this thesis, as this thesis is trying to answer if bottom trawling for sand eels can be a reason behind some of the detected seepages in the North Sea. For this investigation Sentinel-1 SAR images of three separate areas of interest together coinciding with wind data and trawling tracks is used. The trawling date and positional data has been provided by The Norwegian Directorate of Fisheries. This data contains information on all reported trawling activity from the beginning of 2020 until late 2021. Two sources of wind data is used in this thesis. First is a three hour average from the Ekofisk weather station, and secondly the SAR wind calculated for each separate image. The oil spills are manually delineated, and from these observations combined with the complementary wind and trawling information oil observations statistics is derived. The statistics of the number of observations are based on a null hypothesis that neither favours observation of an oil slick during or outside of sand eel trawling season. Firstly this thesis will focus on the background that enables the use of SAR to detect oil, then discuss the data and areas of interest, the method, and finally the results.

/ 2

Background

To understand how we can detect oil with the help of SAR it is necessary to discuss some of the underlying concepts that are applied to radar. The following sections will discuss the basics, and how they are applied to create SAR images with a high resolution.

2.1 Radar

The fundamental theory behind radar is transmitting an electromagnetic wave, and the radar equation 2.1 describes the variables that impact the dynamics of a radar system.

$$P_r = \frac{P_t G_t}{4\pi R^2} \frac{\sigma}{4\pi R^2} A_e \quad (2.1)$$

The left hand P_r is the received signal power. The first or left-most factor on the right-hand side describes the power density at a distance R meters from a radar that radiates with power of P_t watts from an antenna of gain G_t [19]. The second factor or right-most factor on the right-hand side is the cross section σ of the target in square meters. Finally A_e is the effective area of the radar receiving antenna.

2.2 Electromagnetic Waves

Electromagnetic (EM) waves are waves that do not need a medium to propagate through space. They are a form of radiation that travels throughout the universe at the speed of light. An electric wave is coupled with a magnetic wave that is transverse and can have different polarization, frequency, intensity and phase [2]. For SAR a specific range of frequencies are preferred, and these frequencies are shown in Table 2.1 and will also be discussed in more detail in section 2.2.1.

2.2.1 Frequency bands and corresponding applications

Most of the electromagnetic waves in the infrared spectrum are absorbed in the atmosphere. On the other hand, microwaves are transparent in the atmosphere, and won't be affected by variables such as clouds and sunlight [3]. In other words, meaning that microwaves pass through the atmosphere and can be transmitted and received when sending signals to the Earth from a satellite. The microwave frequencies have been split into different bands that are commonly used for SAR. These frequency regions are defined in Table 2.1. X- and C-bands are the most commonly used bands for ocean surface monitoring, such as ocean oil spill monitoring and sea ice monitoring. For land monitoring, requiring deeper penetration into leaves and other vegetation, longer wavelengths such as the L-band and P-bands are used. These wavelengths will scatter and interact with leaves and tree trunks. While shorter wavelengths such as the X-band will mostly interact with the leaves, or in the case of marine monitoring the ocean surface, ice, and vessels. The European Space Agency (ESA) Sentinel-1 mission uses SAR instruments for earth observation, which operates with C-band frequencies.

Table 2.1: Overview of the different bands, showing their associated frequency, wavelength, and the application typical for that band [4].

Band	Frequency	Wavelength	Application
X	8 – 12 GHz	3.8 – 2.4 cm	Urban monitoring, ice and snow
C	4 – 8 GHz	7.5 – 3.8 cm	Ice, ocean maritime navigation
S	2 – 4 GHz	15 – 7.5 cm	Agriculture monitoring
L	1 – 2 GHz	30 – 15 cm	Biomass and vegetation mapping
P	0.3 – 1 GHz	100 – 30 cm	Vegetation mapping and assessment

2.2.2 Polarization of electromagnetic waves

Electromagnetic waves can be polarized in three different ways. The different types of polarization are linear, circular, and elliptical. The SAR instruments

typically use linearly polarized electromagnetic waves, and Figure 2.1 shows a vertical and horizontally polarized EM wave.

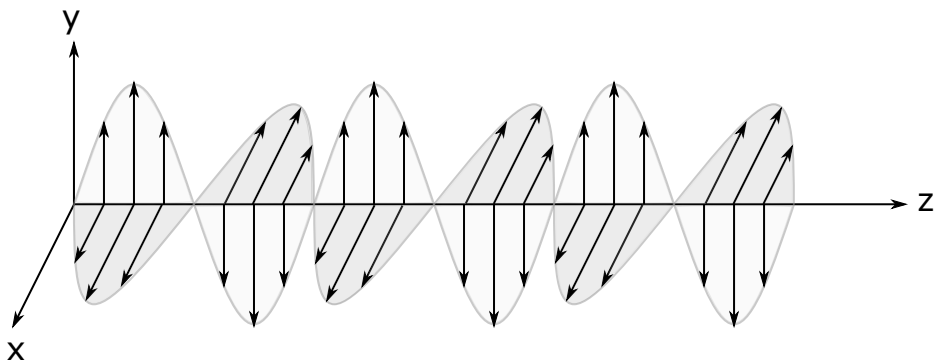


Figure 2.1: Illustration of a vertically polarized wave along the y-z plane, and a horizontally polarized wave along the x-z plane.

A single-polarization system transmits and receives a single polarization in the same direction. Typically classified as a vertical-vertical (VV) or horizontal-horizontal (HH) polarization. A dual polarization system transmits in a single polarization (V or H), and receives in both vertical and horizontal (V and H). This results in VV and vertical-horizontal (VH) polarization, or a horizontal-vertical (HV) and HH polarization data. A quad-polarization system will transmit and receive in both polarizations, and contains information from all polarizations.

2.2.3 Signal and noise in radars

When a radar signal is transmitted and subsequently interacts with the object at a distance R, the returning and received pulse will always include some degree or magnitude of noise. In order to determine variables such as the relative thickness of an oil spill the strength of the received signal must be stronger than the noise. This is known and denoted as the signal-to-noise ratio (SNR). When the signal power received (P_r) is equal to the power of the noise (P_n) the SNR equals 1. SNR can also be described as a measure of quality in which values larger than or much larger than 1 would indicate that the signal is very distinguishable from the background noise. On the contrary, values less than 1 reduces the ability to distinguish the transmitted signal from the thermal noise.

2.3 Synthetic Aperture Radar (SAR)

SAR is an alternative to Real Aperture Radar (RAR). Satellites and other air-borne carriers have a restriction in size, and for having sufficient resolutions the antenna on a RAR would need to be larger than what is possible to design on a satellite. Without a big enough antenna the resolution will be reduced, and the solution is to use a smaller antenna and mimic the effect of a larger antenna, where the forward motion of the satellite in the flight direction is used to synthesize a larger aperture than the physical aperture on the satellite. Figure 2.2 illustrates the synthetic aperture principle that increases the antenna size synthetically.

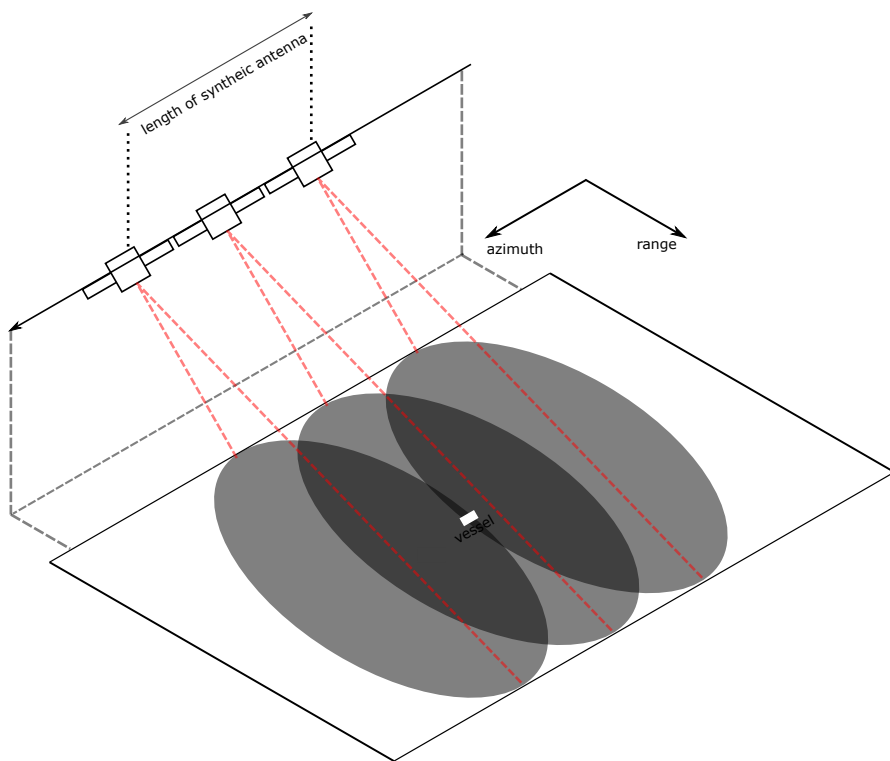


Figure 2.2: As the satellite moves in the azimuth direction it makes multiple observations along the path. The first observation has the vessel at the edge of the observation. The middle observation has the vessel at the center, and finally the last observation is done just as it leaves the view of the satellite. If the vessel is standing still, the length of the synthetic antenna is the distance from the first to the last observation.

The signal received by a SAR vary in strength depending on different factors, such as the small-scale roughness and relative permittivity properties ([3]). The transmitted signal has parameters such as frequency, polarization, power and phase that together can be used to create an image of the observed area.

Equation 2.2 is the SAR spatial resolution in the azimuth direction (along flight direction) where D is the antenna length.

$$X_a = \frac{D}{2} \quad (2.2)$$

In the side-looking or range direction, perpendicular to the azimuth direction, looking away from the satellite, another technique has to be applied. For a single frequency pulse the resolution decreases as the pulse length increases. We want longer pulses so that we can transmit more energy, but we also want a high resolution in range. Here we can use a chirp, which is a frequency modulated pulse. A chirped signal can be combined with pulses that are much longer, which allows for more energy or higher signal strength to be transmitted and then received. The chirped signal can be processed when received to correlate with the transmitted pulse, and then achieve a high resolution in range. Equation 2.3 is the spatial resolution in range where c is the speed of light, τ is the pulse length and Φ is the incidence angle.

$$X_r = \frac{c\tau}{2 \sin \Phi} \quad (2.3)$$

2.3.1 SAR incidence angle

From equation 2.1 we can see that the received signal power is reduced as the distance traveled by the signal increases. The reduction in the received signal power is approximately exponential in power, and linear in decibels. As such, the SNR is reduced with increased incidence angle. Figure 2.3 shows the geometry that results in a brighter image in near range, and a darker image in far range. Figure 2.4 shows this phenomena in a SAR image. SAR images in operational systems will have a limit for incidence angles.

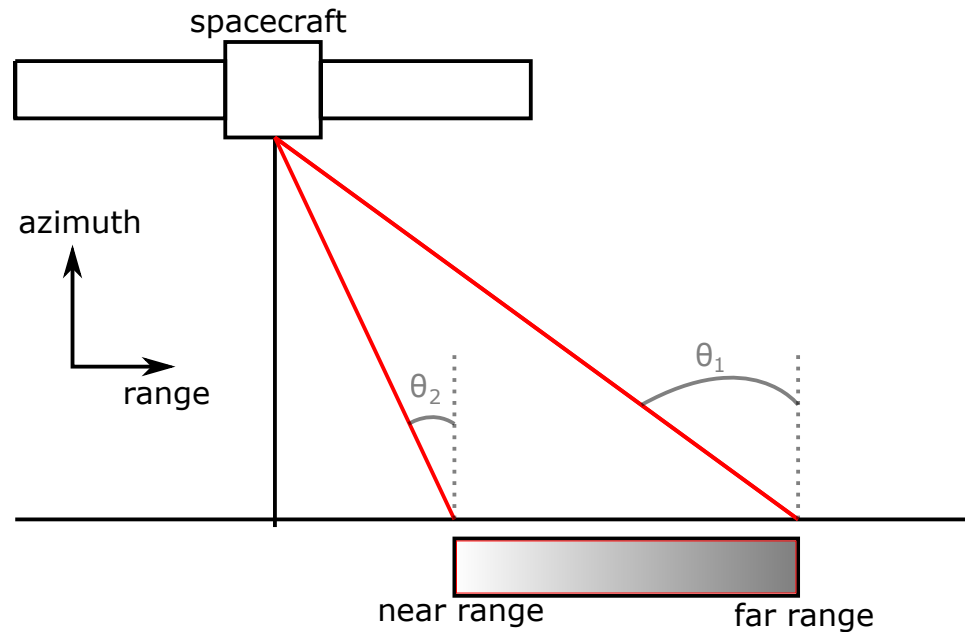


Figure 2.3: Illustration of how the incidence angle impacts the return signal. For low incidence angle θ_2 the backscattered signal has a higher return. In far range for incidence angle θ_1 the signal is lower and therefore darker.

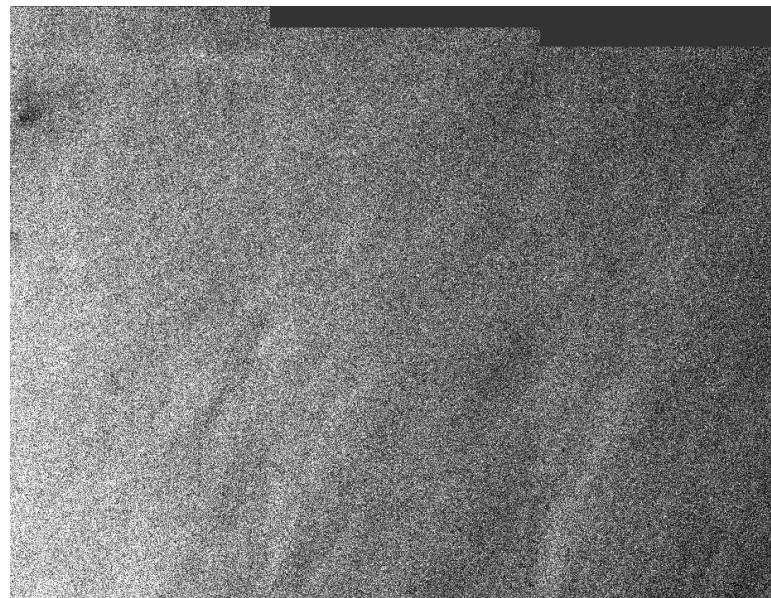


Figure 2.4: Sentinel-1A image from 2020.05.24 that shows the phenomena of a higher backscatter power in near range (left side of image), while less backscatter power in far range (right side of image). The image contains open water.

Oil is a target that has a low amount of backscatter signal (which will be discussed more in section 3), and can be impacted by noise contamination. For the Co-polarization channels HH, and VV the backscatter value is higher than for the cross-polarization channels VH, and HV. The cross-polarization channels will therefore have a higher noise contamination, which will impact the ability to determine regions of thicker oil. The SNR will decrease quicker in the cross-polarization channels, which will mean that low backscatter targets such as oil will have a low SNR [3]. If the oil slick is below the noise floor the slick may be possible to detect, but not characterize.

2.3.2 Pre-processing and calibration

A SAR image can be processed differently depending on the needs of the user. A typical useful processing step is to try and reduce the amount of speckle noise. Speckle noise or salt and pepper noise can appear as granular noise, resulting from constructive and destructive interference of the signal [10]. One possibility to reduce noise is to average several images over the same area [20].

Calibration

Calibration is used to qualitatively define a system response to the known controlled system inputs [8]. This is important when analysing and comparing images.

Sigma nought (σ_0) is a measure of the strength of a radar signal reflected by a distributed scatterer. It compares the strength observed to an expected strength from an area of one square meter [8]. In the same sense the Noise Equivalent Sigma Zero (NESZ) is a measure of the backscatter of thermal noise.

For this thesis the work being done is mostly manual and quantitative, and therefore the importance of calibration and noise reductions is absent. Still in other cases, they would be important. While calibrating to sigma nought is useful it will not impact the ability to identify oil slicks.

Speckle (Salt and pepper)

As previously mentioned the speckle noise can appear as a granular noise. Figure 2.5 shows an image that has been calibrated to Sigma nought. The image shows a granular noise that has pixels of increased values.



Figure 2.5: A Sentinel-1A image from 2020-04-18 calibrated to Sigma zero. The bright spot is a vessel with a wake. The brighter tail behind is the turbulent wake as the ship moves through a low wind ocean.

Multi-look

Multi-look can be used as an averaging filter, to reduce the noise but at the cost of pixel resolution. This takes a $N \times N$ pixel grid and averages the value to one pixel over the entire image. Figure 2.6 shows a 5×5 multi-looked image. The image appears smoother when compared to only the sigma nought version, and has therefore reduced the amount of speckle noise at the cost of resolution.



Figure 2.6: A Sentinel-1A image from 2020-04-18 calibrated to Sigma zero with a 5x5 multi-looked window. The image is the same as seen in Figure 2.5.

/ 3

SAR Imaging for marine surface oil slick detection

In Figure 3.1 we can see an example of how marine surface oil slicks reduce the backscatter radar signature and results in dark areas compared to the rest of the ocean surface. The use of satellite SAR allows us to have periodic monitoring of the ocean surface, and to monitor ongoing oil spills airborne SAR provides quicker repeat observations. In this chapter we will look at what makes it possible to detect oil spills with SAR, the benefits and advantages of SAR, and the included challenges.

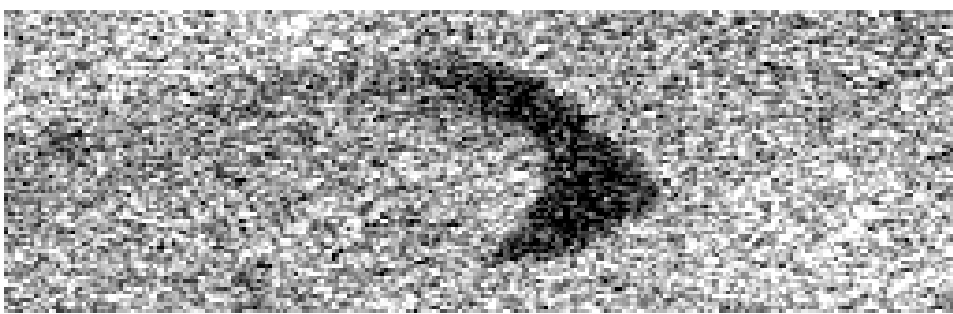


Figure 3.1: Example image of surface slicks observed in a Sentinel-1A image from the 7th of May 2020.

For SAR imaging and slick detection we need a method for differentiating a slick from the surrounding open sea. One factor is the characteristics of the interaction between oil and water. Oil has a lower density than water, though a higher viscosity, and will float at the ocean surface. This oil film spreads out over the ocean surface due to wind and weather interactions. The higher viscosity in oil creates a dampening of typical ocean wave structures such as capillary waves and gravity waves. The small-scale roughness of the ocean surface is subsequently reduced which reduces the backscattered signal, and the resulting oil detection appears as a dark spot in the SAR image. This is clearly visualised in Figure 3.3 where we can see how marine surface oil slicks reduce the backscatter radar signature and results in dark areas compared to the rest of the ocean surface.

3.1 Advantage of using SAR for oil slick monitoring

Not including the apparent ability of SAR imaging to differentiate oil spills from ocean water in Figure 3.1, there are multiple strengths of the SAR imaging. Many of these strengths are amplified when applied in Norway due to frequent cloudy or foggy weather and lack of daylight for longer periods of time at certain times of the year. Optical imaging is reliant on being operated during day time for the sun to illuminate the ocean surface and reflect light towards the camera, and need low cloud coverage. As mentioned in chapter 2, because SAR satellites do not rely on light, and can see through the atmosphere and clouds, these problems are not an issue, and this means that SAR is more suitable for all day monitoring.

3.2 Challenges or disadvantages

As with most instruments, even though they have some strength, the SAR also has some weaknesses and limitations. The Bonn Agreement Oil Appearance Code is a classification of the thickness of the oil based on optical observations [1]. Table 3.1 shows how the color of the oil will change depending on the layer thickness, and the code was designed for fresh oil, i.e. oil that has not emulsified. As the Bonn Agreement relies on optical observations it relies on optical images. For SAR we can only identify the relative thickness within a scene by using the damping ratio to determine areas of increased damping (discussed in more detail in [3]), not the actual thickness of the spill and as it is scene specific the derived values can not be compared with another image. However, relative

thickness is still a useful parameter to calculate for one image as long as the power of the signal is greater than the noise. In oil spills it is common to assume that 90 % of all oil volume is within 10 % of the total surface area, therefore the relative thickness can be used in cleanup to identify a region in the slick that contains most of the oil.

Table 3.1: Boon Agreement Oil Appearance Code labels that show the layer thickness and volume related to each specific code. Commonly used for optical oil classification.

Code	Description - Appearance	Layer Thickness Interval (μm)	Litres per km^2
1	Sheen (silvery/gray)	0.04 to 0.30	40-300
2	Rainbow	0.30 to 5.0	300-5000
3	Metallic	5.0 to 50	5000-50,000
4	Discontinuous True Oil Color	50 to 200	50,000 - 200,000
5	Continuous True Oil Color	≥ 200	$\geq 200,000$

The usual orbit around the earth for a satellite in Low earth orbit (LEO) is around 100 minutes [6]. Therefore another challenge with satellite SAR is the repeat observation time. One satellite is limited by its orbit time, and the rotation of Earth. In the case of Sentinel-1A and Sentinel-1B they had a repeat observation time of six days.

When analysing a SAR image for oil detection knowledge of oil spill lookalikes are essential. Many phenomena that can occur on the ocean surface, such as algae, low wind, and weather phenomena can look similar to an actual oil spill. Figure 3.2 shows an image with dark areas where the wind speed is generally too low to identify any dampening from an oil slick.

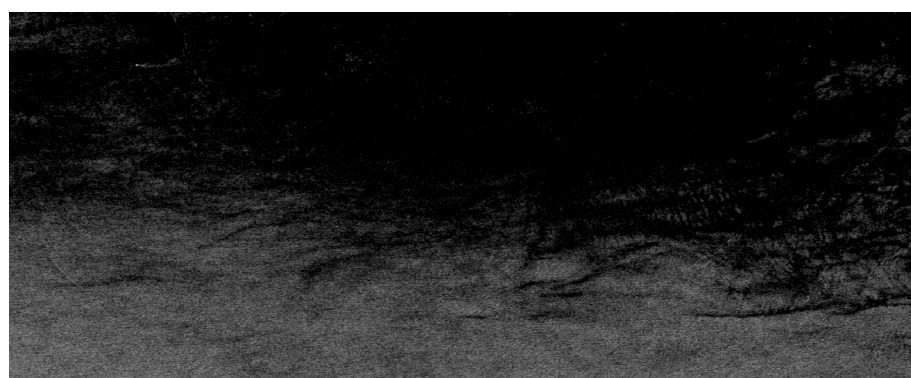


Figure 3.2: Image taken by Sentinel-1A 2020.06.10. The dark section in the north is an area of low wind speeds. The image has been calibrated to sigma nought, and multi-looked with a 3x3 window.

3.3 Theory for differentiating open sea and oil slick

In this section I will present the theory behind SAR imaging and the technicalities that makes it possible to differentiate between open sea and oil slicks.

3.3.1 Scattering mechanisms

When the SAR transmitted signal interacts with a surface the signal scatters. If we have a perfectly smooth surface the signal will be reflected in the specular direction of the signal. In this case, the satellite will not receive any backscattered signal, and it will appear as darker areas in a SAR image. If the surface is semi-rough most of the signal will scatter in the specular direction as coherent scattering, but it will also include a diffuse scattering component. This diffuse scattering will be returned back to the satellite and this surface will appear brighter in the SAR image. This is already seen in Figure 3.1 where we have very dark features as a result of a damped ocean surface. The surrounding ocean is comparably rougher than the dark spots and appears brighter. As the roughness increases the scattering in the specular direction decreases. Figure 3.3 shows how oil impacts the backscattered power and dampening of the small-scale roughness on the ocean surface.

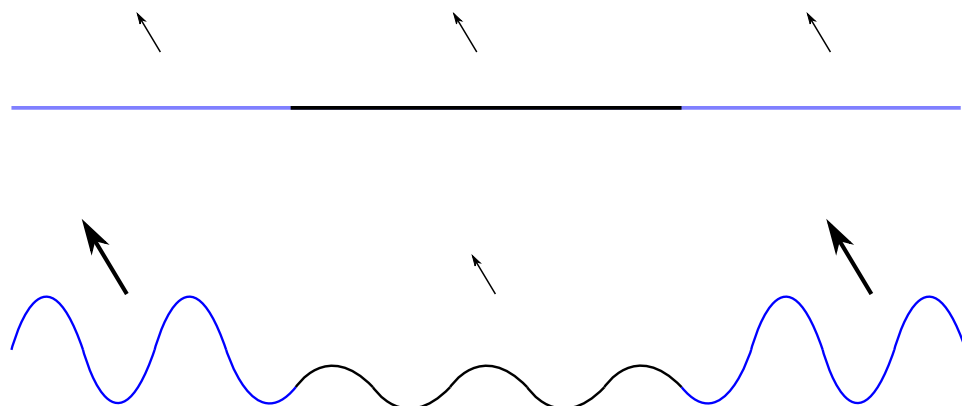


Figure 3.3: In the top illustration the power of the backscattered signal is illustrated as equally sized arrows. The arrows show how it would be difficult to differentiate oil and the areas of calm ocean due to low wind. While the bottom shows an increase in backscatter of areas of high wind and rough ocean. The oil dampens the ocean waves and creates an area of lower power backscatter. (The arrows only illustrate how the surface of the ocean impacts backscattered power, and should not be used as a comparison between scenarios.)

3.3.2 Relative permittivity (Dielectric constant)

A dielectric is an insulating material, and the insulating materials ability to store electric energy in an electric field is given by the relative permittivity. The relative permittivity is given as the ratio of the permittivity of a material and the electric permittivity of a vacuum.

Equation 3.1 defines the relative permittivity ϵ_r as a complex number where the vacuum permittivity is given as ϵ_0 , the real part as ϵ' and the complex part as ϵ'' .

$$\epsilon_r(\omega) = (\epsilon'(\omega) - i\epsilon''(\omega))/\epsilon_0 \quad (3.1)$$

The interaction of the electromagnetic wave and the surface is impacted by the relative permittivity of the surface. A thick layer of oil will have a lower relative permittivity than a thin film of oil. The relative permittivity is dependent on temperature T, and salinity S. The dependence on salinity means that the value depends on the location of the ocean. A typical value for sea water in the North Sea is $\epsilon_r^{SW} = 75.4 - i59.4$ (for 1.26 GHz (L-band)) [15], when compared to the value for oil $\epsilon_r^O = 2.3 - i0.02$ [17] it is clear that the relative permittivity for oil is much lower than for sea water.

The relative permittivity and the scattering mechanics will together impact the backscattered power. In short, both these phenomena are important factors for creating discernible dark spots in SAR images.

Since the relative permittivity is dependent on the angular frequency it is dependent on the frequency of the transmitted radar wave. A lower relative permittivity means that the amount of total energy reflected by the surface is reduced, hence meaning that the total energy reflected back from the surface makes it appear darker in the SAR image.

3.3.3 Wind

Wind speeds also impact the detection capability for marine oil slicks and seepages. Higher wind speeds create a roughened surface in the oil slicks such that it blends together with its nearby environment. Consequently, higher wind speeds makes it more challenging to detect and identify slicks. At the same time will absence of wind results in a flat and even surface regardless of oil on the surface of the water or not, making it difficult to separate from the open water and the oil slick and its surrounding ocean surface will look the same.

The wind speed range most suitable for oil spill detection is between 2 and 12 m/s [9], as these wind speeds will create backscatter damping that enables SAR to separate oil slicks from clean sea. The optimal wind speeds are not hard limits, but can vary slightly.

During the winter months the wind speeds along the Norwegian coast on the ocean surface are higher than during the summer months, indicating that fewer slicks are generally detectable during the winter months in Norway.

/ 4

Study areas and data sets

The areas of interest (AOI) for study in this thesis are located in the southern part of the North Sea. The Norwegian Petroleum Directorate (NPD) have created a grid of blocks that geographically divide sea areas within the Norway Exclusive Economic Zone (EEZ). These blocks have been used to create three larger AOI. Each area will be investigated for two years, 2020 and 2021. This means that in total there will be six sets of data.

Information on the locations of bottom-trawling vessels combined with satellite images are used as foundation to investigate whether there is a possible connection between bottom trawling and natural oil seepages. In Figure 4.1 we can see the coast of Norway and Denmark, and the EEZ of Norway. Each square is the blocks used by NPD, and the larger filled squares in red, orange and green is the respective AOI.

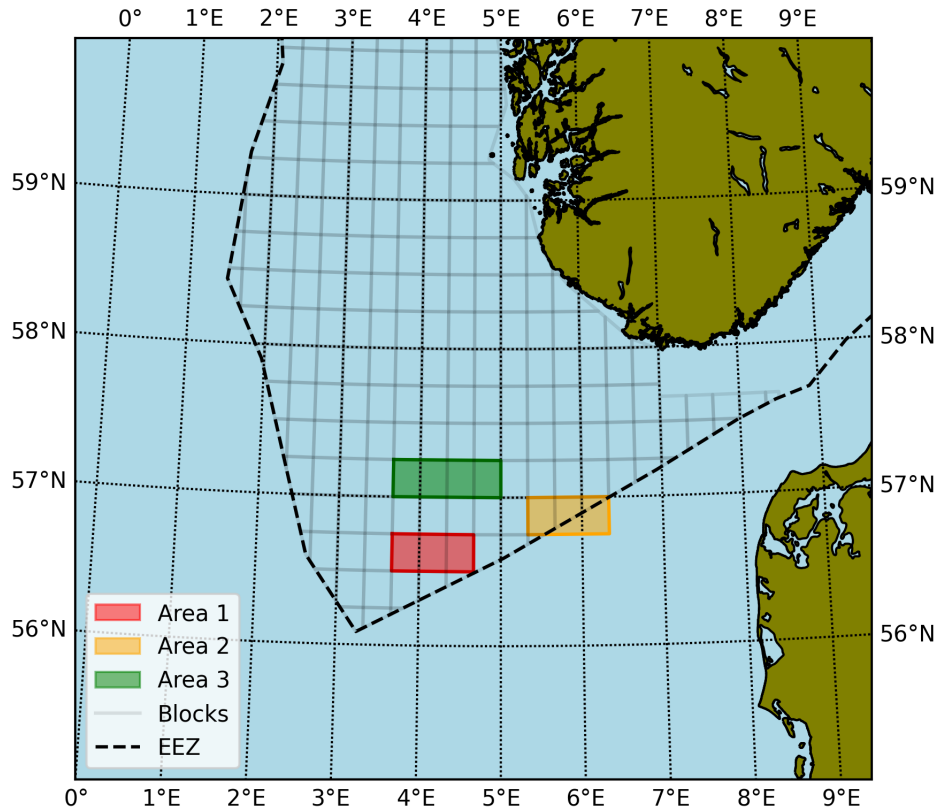


Figure 4.1: Map showing Area 1 in red, Area 2 in orange, and Area 3 in green. The dotted line is the EEZ of Norway. The blocks are used by NPD as a geographical unit for division in the petroleum sector on the Norwegian continental shelf.

4.1 Sand eel fishing - bottom trawling

Sand eel is a fish with a slim torpedo shaped body which makes it adept at burrowing in sandy sea beds. It spends most of its time in burrowed state, and therefore a common fishing method is trawling the sea bed. In the winter it hibernates, but it is also a winter spawner and has to exit hibernation around new years. The grazing period for this fish varies between old and young fish, but starts in April and lasts until July [11].

The sand eel fishing season is seasonal and starts the 15th of April and lasts until the 23rd of June in Norway [11]. The fishing period forms the basis of the time series investigated, and in addition to this we are also interested in some

data before and after the season, to statistically determine whether the bottom trawling is the main reason behind the natural seepages. The rationale being that the bottom trawling also dredges or digs up oil from the seafloor as an added consequence of fishing. Table (4.1) shows an overview of the timetable and information regarding the data that is being investigated.

Table 4.1: Overview of the data used for this thesis, date, the mode and which satellite acquired the data.

Start date (dd/mm)	01.04
End date (dd/mm)	31.08
Years	2021, 2020
Satellites	Sentinel-1A, Sentinel-1B
Mode	Interferometric Wide (IW)

4.2 Sentinel-1

This thesis will rely on the commercially available data supplied by ESA and their Sentinel-1 satellites. Sentinel-1A is currently active and was launched on the 3rd April 2014. Sentinel-1B was launched 25th April 2016, but unfortunately ended its mission in early 2022 [7]. Both satellites operate in a near polar, sun-synchronous orbit with a repeat cycle that takes 12 days for one satellite.

Sentinel-1 has 4 different acquisition modes. For this thesis the data we use the Interferometric Wide Swath (IW) mode. This is the main acquisition mode used over land and coastal waters, and for coastal waters VV + VH is the most commonly used band combination. Table 4.2 gives an overview of specifications for this mode.

Table 4.2: List of characteristics of Sentinel-1 IW acquisition mode.

Characteristic	Value
Swath width	250 km
Incidence angle range	29.1° – 46.0°
Polarisation options	HH + HV, VV + VH, HH,VV
Maximum Noise Equivalent Sigma Zero (NESZ)	-22 dB
Spatial resolution	20 m Range, 22 m Azimuth
Pixel spacing	10 m Range, 10 m Azimuth

4.2.1 Acquisition modes of Sentinel-1

The aforementioned Sentinel-1 operates in four acquisition modes: Stripmap (SM), Interferometric Wide swath (IW), Extra-Wide swath (EW), and Wave (WV) [5]. Figure 4.2 shows the different modes and the specifications such as swath width, and incidence angle range.

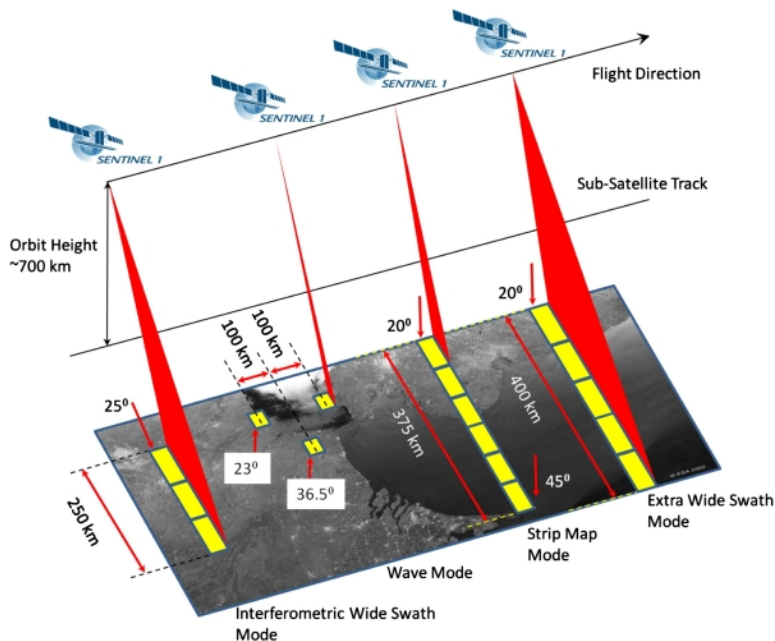


Figure 4.2: Illustration of the geometry of the different acquisition modes [5]. Copyright: European Space Agency - ESA

However, as illustrated in Figure 4.2 most of the scan modes of Sentinel-1 are restricted in the incidence angles, such that the backscattered power is not too high or too low.

4.3 Wind data

As already mentioned, if the wind speeds are too high or low it becomes almost impossible to detect any man-made slicks or natural seepages. In order to detect slicks with SAR images we need to define a range of wind speeds that allows the slicks to dampen the natural sea roughness due to wind and wave interactions [9]. As such, wind speeds will be used as a measure of reliability of the oil slick measures and to limit the data we look at. There will be two sources for

the wind data, one is from the weather station on Ekofisk, the second will be retrieved from SAR wind for each image. The distance from Ekofisk weather station and the areas of interest can be a challenge since wind conditions can change over distance. The inclusion of SAR wind will provide a local estimation of wind speeds, and can be an additional source of data when analysing larger datasets.

Figure 4.3 shows a boxplot of the wind speeds for each month. The data points are from the closest three hour average of an image. While the wind speeds in June for 2020 had an average above May and June, the total average increases for the months outside the summer months.

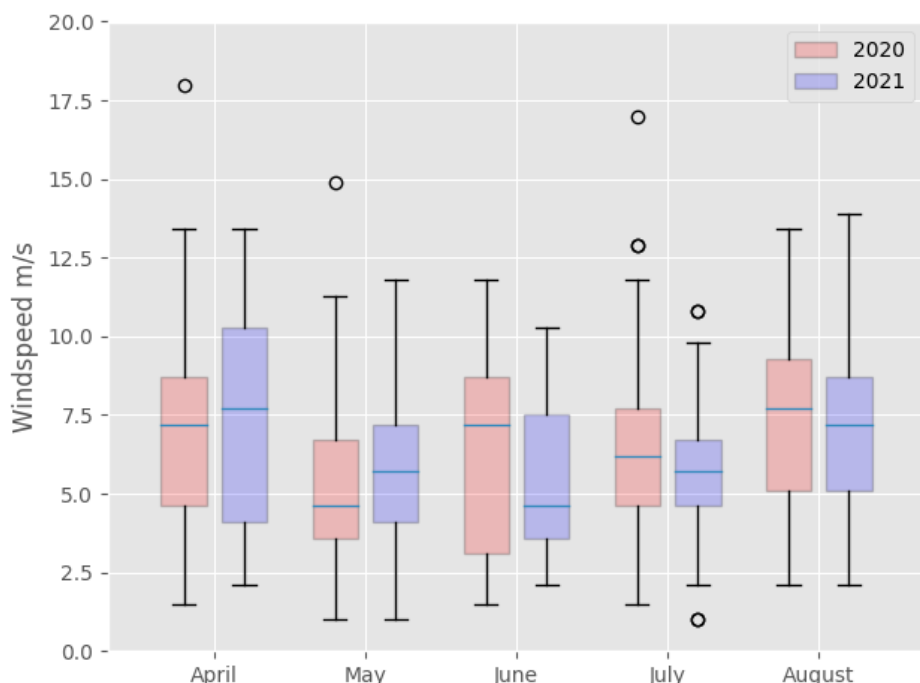


Figure 4.3: Wind speed values from Ekofisk to illustrate the range of wind speeds for each month.

4.4 Fishing boat tracks

In order to track and monitor ocean activity, the vessels are equipped with Automatic Identity System (AIS) transponders. Vessels are required to have such a transponder onboard if the vessel is larger than 15 m, or the Norwegian Directorate of Fisheries have required AIS for vessels fishing for certain species

of fish [14].

The data positional data received from the AIS is important to identify if observations done in a SAR image is a result of trawling activity. The data used in this thesis was received from the Norwegian Directorate of Fisheries. The data contains trawling activity from 02.01.2020, to 01.08.2021, constrained between approximately 56.5 °N-58 °N and 3.5 °E-6.5 °E.

Figure 4.4 shows all tracks together with all areas of interest. Each vessel track has been time stamped with a date, but not the specific time of the day. Therefore our precision is limited to only compare the tracks from the same day as the SAR image. Specifically, we cannot determine if the vessel was nearby before or after the image. As most of the SAR images are acquired around 6 UTC and 18 UTC there might be up to a 18h time gap between the ship track and the SAR image.

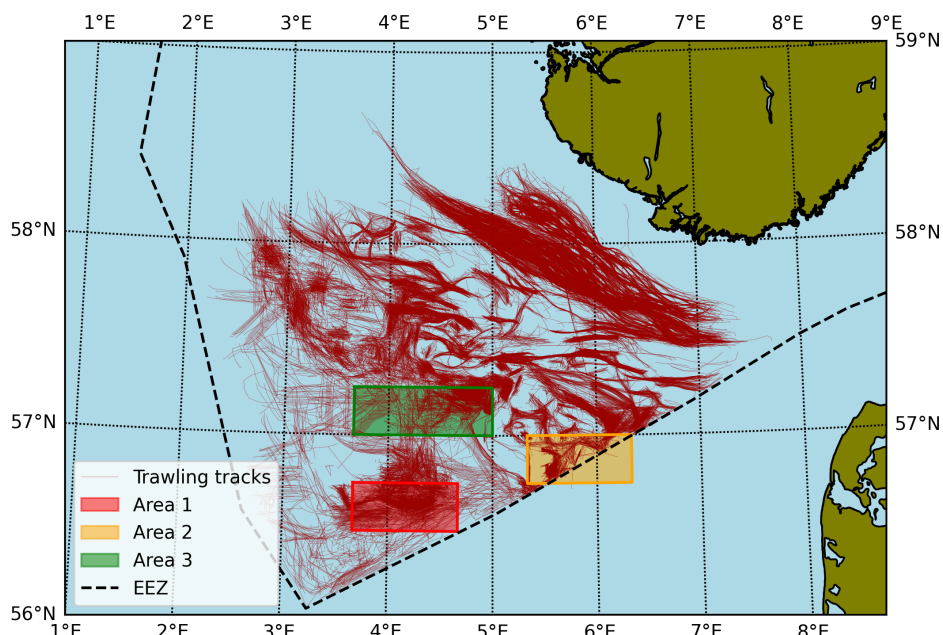


Figure 4.4: Illustration of all 29000 trawling tracks from 2020 to 2021 in red. The density of trawlers varies, but Area 1, Area 2, and Area 3 have areas of increased trawling activity.

/ 5

Method

This chapter will discuss the methods for data handling, analysis of images, and further data processing to investigate the hypothesis.

5.1 SAR data

The data used for this thesis has been downloaded by searching for Sentinel-1 SAR images that cover each area in Figure 4.1. The data has then been subsetted to each AOI after processing the data with SeNtinel's Application Platform (SNAP). The images have been calibrated to sigma nought, and converted to decibels. For the manual analysis, geocoding and subsetting the scenes have the most impact on the workflow.

5.1.1 Subsetting

To reduce the size of each image the scenes have been reduced to the AOIs. This is done by cropping the image to a predefined Well-Known Text (WKT) file that contains the perimeter of each AOI.

5.1.2 Geocoding

To be able to analyse distances, positions and other statistics the subsetted images were geocoded to the same coordinate system, here the World Geodetic System (WGS) WGS84. This coordinate system is going to be the basis for the delineation of oil slicks.

5.1.3 Delineation

Attempts were made in this thesis work to use a semi-automatic delineation algorithm to decrease the workload needed to analyse a large data set. This proved to have some challenges, the data that had been downloaded had already been pre-processed with an increase in gain in certain areas of the images. Hence, this idea was abandoned in favor of a fully manual approach, but it can still be used operationally. The manual delineation has been done for each image where an oil spill has been detected. A shapefile for each image has been created, where each shapefile could contain multiple polygons. The delineation has been done without auxiliary wind data, or with assistance of trawling tracks, both of which are normally used to aid the operational oil spill detection services. Some images will have more challenging lookalikes and natural phenomena as discussed in section 3.2. For challenging images the author has gathered a second opinion.

Some images will have multiple observations, and therefore multiple polygons drawn for each slick. For all images they will either be classified as an image with or without an observation regardless of the number of observations.

5.2 Wind data

As discussed earlier wind will affect the possibility to detect slicks on the ocean surface, and two different sources have been used to compare wind speeds.

5.2.1 Ekofisk

Unfortunately there is no nearby weather station to the AOIs. The closest one, Ekofisk, was chosen as a source for the wind data. The wind sensor on Ekofisk is located at 58 meters above sea level. The wind speeds available are a three hour average, eight times per day. All SAR images have been matched with the closest wind measurement. The height of the wind measurement station can

be a challenge as it is not going to represent the wind conditions at the ocean surface.

5.2.2 SAR wind

SAR wind can be calculated with SNAP. The module wind field estimation is based on the CMOD5 model for wind field estimation described in more detail in [12]. The wind direction is not used within this thesis. A window size of 4km has been used to get wind points for even all images. The window size determines the size of grids the image will be divided into. Each grid will provide a wind speed value. This gives multiple points for the wind data, but will be averaged for simplicity. For some images that are very small this method will not generate wind data.

/ 6

Results and discussion

In this section we present the results and statistics from analysing trawling activity and oil spill observations as discussed in chapter 5. The data and results presented aim to try and identify if bottom trawling for sand eels can be a cause for some of the detected oil seepages in the North Sea. Additional supportive figures can be found in the appendix A.1.1. The presence of oil slicks has been assessed for time of year, reoccurring location and distance to closest trawling track.

6.1 Number of observations and amount of trawling activity

Table 6.1 shows the total number of images from Sentinel-1A and 1B for each area, the number of observations for each area, and the percentage of images with observations. The total number of observations in 2020 is greater than in 2021. We will later discuss if the increase in observations for 2020 may be a result of increased trawling activity that year.

Table 6.1: Overview of the number of images and the number of observations for each area in 2020 and 2021.

2020	Total images	Number of images with observations	Percentage of images with observations
Area 1	137	38	27.74 %
Area 2	153	28	18.3 %
Area 3	134	15	11.19 %
2021			
Area 1	149	15	10.07 %
Area 2	145	7	4.83 %
Area 3	164	23	14.02 %

Figure 6.1 shows the number of trawling tracks for each day. The vertical dashed lines in green and red indicate the start and stop of the sand eel fishing season in 2020, while the dotted lines are for the year 2021.

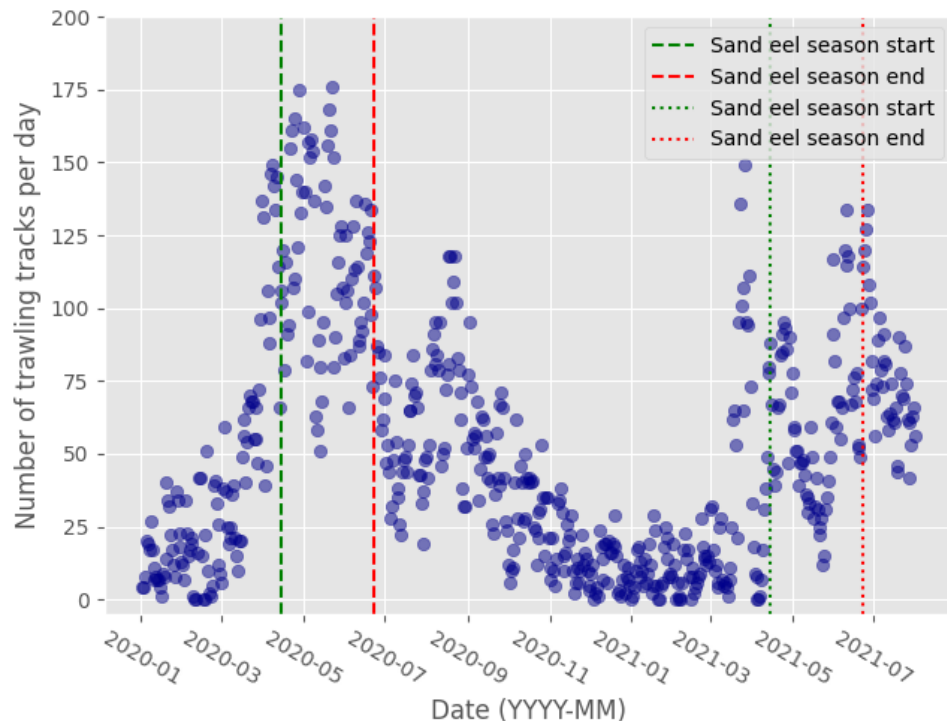


Figure 6.1: Graph of the number of trawlers per day. Outside the Sand eel season there is a big drop in number of tracks per day. When comparing the Sand eel season in 2020 and 2021 there seems to be decrease in activity in 2021.

From the figure it is clear that there was less trawling activity during the 2021

season compared to the 2020 season. This is also seen in Table 6.2, which shows that the total number of trawling tracks during the 2020 season is almost double when compared to the 2021 season.

Table 6.2: Total number of trawling tracks inside the season window in Figure 6.1.

Year	Total trawling tracks
2020	7939
2021	4190

If there was a correlation between bottom trawling and oil slick observation we would expect that we have less observations if the bottom trawling activity decreased. From Figure 6.1, and Tables 6.2 and 6.1, both the number of oil seepage observations and the number of bottom trawling tracks are greater in 2020 compared to 2021. The decreased number of trawling tracks in 2021 is obvious, but the sudden drop in the middle of the season of 2021 in Figure 6.1 is not easily explained from the data alone.

6.2 Observed oil slicks, time of year and wind speed

The wind speed is important for identification of oil slicks on the ocean surface. Figures 6.2 and 6.3 show the distribution of observations with regards to time and wind speed. The suitable wind speed for oil detection is presented in section 4.3. The shaded area in green is for good wind speed, blue for marginal wind speeds, and red is for wind speeds that are considered unfavourable for oil detection.

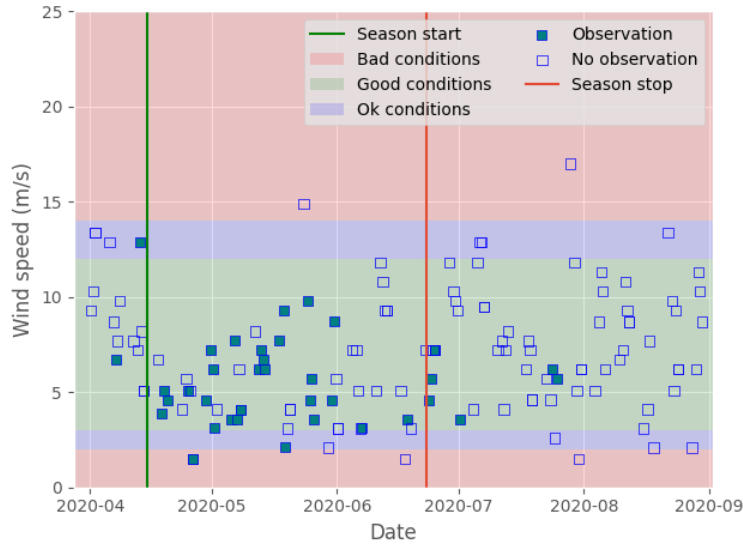


Figure 6.2: Area 1 images with or without observation in 2020 with wind data from Ekofisk.

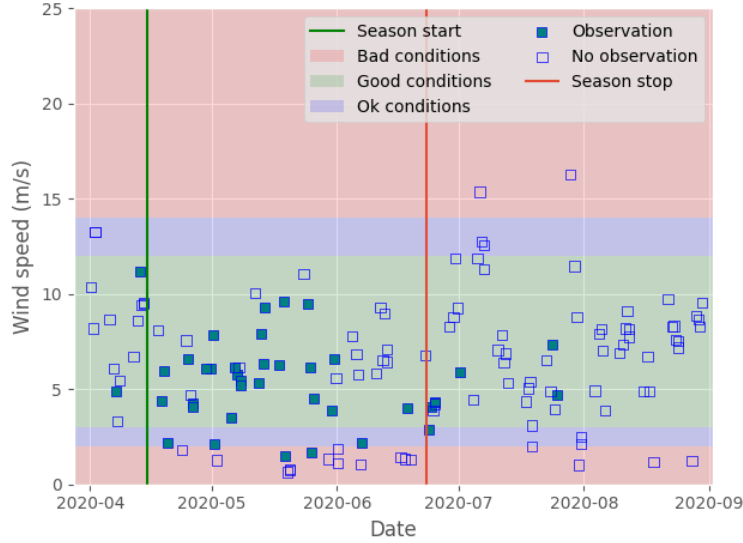


Figure 6.3: Area 1 images with or without observation in 2020 with wind data from SARwind.

For some very small SAR images SAR wind data was not created due to the selected window size discussed in section 5.2.2. Therefore Figure 6.3 will be missing some data points, but they are included in 6.2. The green and red lines

show the start and end of the trawling season. Filled squares denote images with oil observations, while empty squares are images with no oil observations. These figures show how the observations are located in time, and we can therefore identify if there is an increase in observations in the sand eel trawling season.

From Figure 6.2 it is shown that most of the observations occur during the bottom trawling season. The increase in observations can likely be attributed to the increased bottom trawling activity seen in Figure 6.1. In the appendix Figures A.5 through A.10 show the observations of all areas and both years. The observations are plotted with both SAR wind and Ekofisk weather data. The difference in number of observations can be seen over the two years.

6.3 Reoccurring oil slick locations

Figure 6.4 shows the density of observations in the form of a heatmap. If there are multiple overlapping oil polygons they will appear as a more orange-red color. Which means that we have observed oil slicks in the same area at on different images.

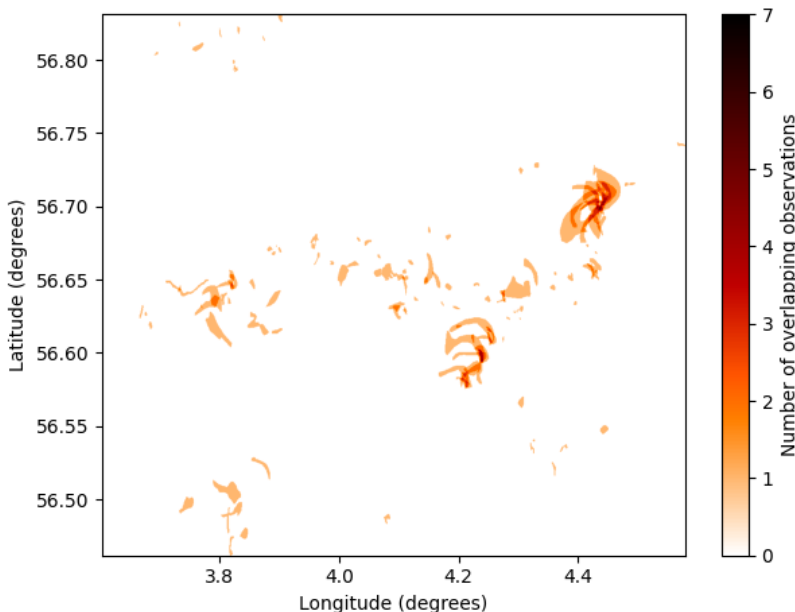


Figure 6.4: All polygons from Area 1 in 2020. Illustrated as a heatmap, and shows any overlapping polygons as a color indicated by the colorbar.

We can see an increase in oil slick observations in some locations of Area 1. At approximately $4.4^{\circ}E$ and $56.70^{\circ}N$ there are 7 overlapping oil observation polygons. Some images have coverage from Sentinel-1A and Sentinel-1B, therefore some slicks can be present in both and drawn twice, although with slight changes due to the phase difference between the satellites.

6.4 Distance to closest trawling track

Figure 6.5 shows each polygon plotted with a color related to the distance to the closest trawler that day. The transparent lines shown are the trawling tracks. Only the trawling tracks from the same day as the observation have been plotted.

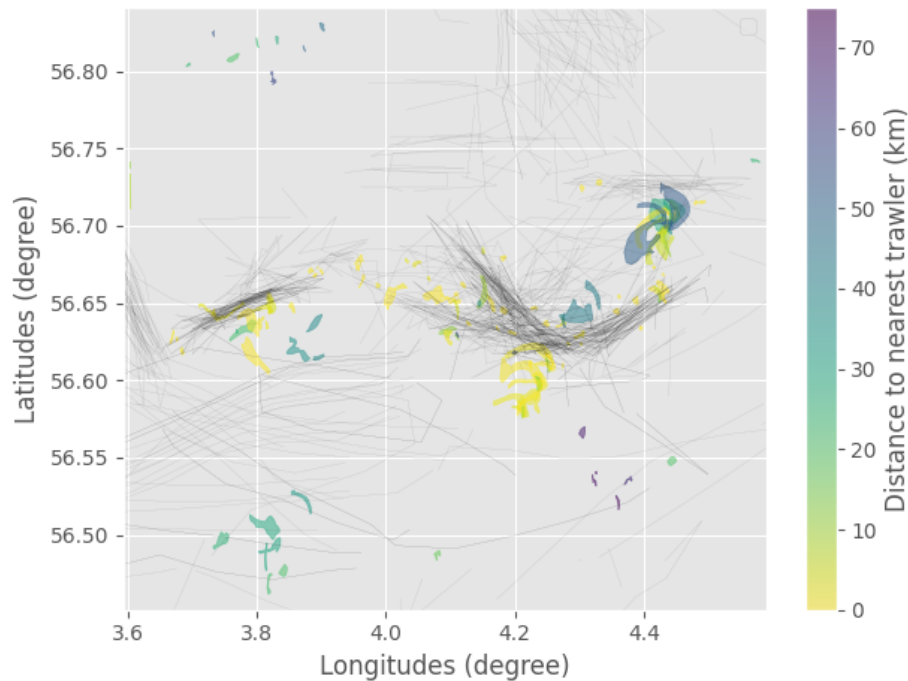


Figure 6.5: Polygons for each slick in 2020 in area 1. The color illustrates the distance away from the nearest trawling track in meters. A yellow polygon has a trawling track from the same day that has been very close, while a dark blue / purple polygon has a trawling track that is further away.

The smallest observations at $4.4^{\circ}E$, $56.70^{\circ}N$ in 6.5 have had trawling activity that has been close to the oil observation polygon. This makes it possible that trawling has triggered a natural seepage that has continued to release over

a longer time. Thus the larger polygons far away from the nearest trawling track would be an old seepage that has been affected by wind and weather conditions. After a closer inspection on the observations at $4.4^{\circ}E$, $56.70^{\circ}N$ and $4.25^{\circ}E$, $56.60^{\circ}N$ they are all observations from 2020.05.05 to the end of May. No observations were made in these locations before or after this period. This lies well within the sand eel season, and the natural seepages could have been triggered by this fishing activity.

In Figures A.18 and A.19 the density of trawling tracks is much lower than in Figures 6.5 and A.16. The reduced number of trawling tracks can be confirmed studying Figure 6.1 and Table 6.2.

6.5 Combined observations

Figures 6.4 and 6.5 shows Area 1 in 2020, with observations in locations with and without increased trawling activity. In some observations the distance to the nearest trawling track is quite large, but this can be a consequence of the trawling tracks only having a date stamp. Since the time of day is not included it is difficult to determine if the slick could have been because of a trawling activity the day before. Similarly it can be difficult to determine if a trawling track was actually after the image time. At $4.4^{\circ}E$, $56.70^{\circ}N$ in Figure 6.5 the darker shapes can be because the slicks have been on the surface for a while and transformed due to weather and ocean conditions. An activity from the day before can therefore be detected a day later and the closest track the day it was detected might not be in the area. Repeat observations will confirm that the source of the observations is from seepages due to the common origin that is visible in Figure 6.4 as a dark spot. In Figure 6.4 we can see two areas of repeat observation at $4.4^{\circ}E$, $56.70^{\circ}N$ and at approximately $4.25^{\circ}E$, $56.60^{\circ}N$. These areas have multiple overlapping polygons, and are repeat observations. From Figure 6.5 we can see that the density of trawling tracks is lower around these observations. This could imply that there is a source for natural occurring seepages in the area.

The same can be seen in Figures A.20 and A.15, there are locations with observations that seem to have the same origin at $4.8^{\circ}E$, $57.12^{\circ}N$, and $4.5^{\circ}E$, $57.20^{\circ}N$. The density of trawling activity tracks is low here when compared to Figure 6.5. The observations have a varying distance to the closest trawler, but could be a result of bottom trawling.

For both Area 1 in 2020 (Figure 6.4) and Area 3 in 2021 (Figure A.15), the observations made have repeated oil observations. For Area 1 in 2021 (Figure A.13) at $4.4^{\circ}E$, $56.70^{\circ}N$ we do not have the same repeat observations, this is

also true for Area 3 in 2020 (Figure A.12). The absence of observations from the same location on different years could be explained by inactivity from the seabed.

There is also the possibility that some trawling activity has not been reported. As mentioned earlier only vessels above 15 m are required to report their position. This means that smaller vessels can be active, without their position being reported. While Norwegian vessels report their catches per day electronically, non-Norwegian vessels only need to report data when they are in Norwegian waters. Hence the trawling data is not entirely complete, and will not show all activity. This can possibly mean that there has been an observation that has a trawling track very far away, but in practice it would be difficult to determine if that is the case.

Figures 6.4 and A.15 show areas of overlapping oil observation polygons. These areas can be repeat observations with short time intervals between two satellite images, or a result of recurring locations of natural seepages that can have been triggered by bottom trawling. From Figures 6.5 and A.20 we can see that areas of overlapping observations have had some trawling activity at approximately 30 km or less. This could imply that the trawling activity along the sea bed can release natural seepages.

The number of observations done inside the trawling season for sand eels compared to outside the season is presented in Table 6.3. This table shows that for 2020 there is a larger number of observations inside the sand eel season. This is supported by the increase in trawling activity seen in Figure 6.1 and Table 6.2. For the year 2021 both Area 1 and Area 2 have approximately 50 % of their observations inside the sand eel season, while Area 3 has a higher portion of observations inside the season. The lower in-season observations in 2021 could be linked to the decrease in trawling activity we see in Figure 6.1 and Table 6.2.

Table 6.3: Overview of the total number of observations for each area in 2020 and 2021. The percentage shows the ratio of images with observation inside the sand eel trawling season to the total number of observations.

2020	Total observations	Total observations in season	Percentage of observations in season	P-value
Area 1	38	30	79 %	0.00024
Area 2	28	21	75 %	0.00627
Area 3	15	11	73 %	0.05923
2021				
Area 1	15	8	53 %	0.49999
Area 2	7	4	57 %	0.5
Area 3	23	16	70 %	0.04656

In Table 6.3 the p-values are presented. They are calculated using a binomial test for each row values, and assume a null hypothesis neither favouring observation of an oil slick during or outside of sand eel trawling season. Meaning that the number of observations inside the sand eel trawling season is 50%. For the test and in line with the thesis hypothesis we used a one-sided test that tested for greater probability of observing oil slicks in trawling seasons. The p-values were considered significant if they were lower than 0.05 per standard convention.

For Area 1 and Area 2 in 2020 the probability of observing oil slicks in the trawling season were significantly more likely than not. This is also true for Area 3 in 2021. From Table 6.3 we can see that the number of total observations are higher for rows with a low p-value. For a higher total number of observations there is generally a larger portion of observations inside the trawling season. For Area 1 and especially Area 2 in 2021 the total number of observations is lower when compared to other rows. This means that observations such as fishing oil outside the trawling season can skew the statistics much more easily when compared to the other rows.

/ 7

Conclusion and future work

The goal of this thesis was to investigate if bottom trawling for sand eels can be a cause for some of the detected oil seepages in the North Sea. This has been done by manually analysing Sentinel-1 images for oil slicks, using auxiliary wind data to identify images with good conditions for oil detection, and trawling tracks to identify if trawling activity has taken place the same day nearby the observation. After investigating three areas in the North Sea over two years, we have discovered that a significant portion of oil slick observations are made inside the sand eel fishing season. For 2020 the total observations was larger than in 2021, and had an average of 76 % observations inside the sand eel fishing season. For Area 1 and Area 2 in 2020 the p-value was below the significance value of 0.05, meaning that the number of observations are likely due to trawling. In 2021 the number of trawling tracks had a sudden drop, and as such the number of observations were much lower compared to the same areas in 2020. For 2021 Areas 1 and 2 had a close to even split of observations inside and outside of the season. Area 3 was an exception in 2021 since it had 70 % of observations inside the sand eel fishing season, and had a p-value below the significance value of 0.05. Area 1 in 2020 had two locations with repeat observations over a month in May. The repeat observations can possibly indicate a source of natural seepages from the sea bed that, has been triggered by trawling activity or just other natural causes that could have increased activity. There are some repeat observations for 2021 in Area 3 that could indicate the

same phenomena. In total our analysis indicates that oil seepages within the three investigated areas could be a result of bottom trawling.

7.1 Future work

In this thesis we have looked at three areas over two years. Sentinel-1 has free and available data from 2014, and gives the possibility to look at many years of trawling activity to try and increase the confidence in trawling activity causing natural seepages. For the two years this thesis has analysed it would seem that there is some correlation, but to reduce the uncertainty a bigger data set is a natural next step.

Another area of improvement is the shortcoming of the trawling data used in this thesis. Only having the date of activity reduces the ability to identify if an observation can be a result of trawling activity only hours before, and makes it impossible to identify if a given trawling track has been made before or after the image time. These shortcomings can be rectified by including timestamps as this enables more accurate identification if trawling is a likely source.

A classification of the type of observation could be useful for measuring the difference between a likely seepage and crude oil from vessels. Recurring seepages in the same location may not be caused by trawling activity, though if seepages only occur during the trawling season it may be easily triggered. For this thesis the shapes of the oil observations have not been considered. A closer analysis on the shapes of oil observations can be used to identify if the source is likely from other activities than trawling. If a long linear feature is discovered it can likely be a result of oil leakage or fishing oil from a vessel. Another method of classifying the observations is by using the relative thickness of the observation to try and identify areas of higher volume oil.

Finally using optical images as a support when available to try and closer identify which type of oil has been observed. This can include some challenges such as weather conditions and may not be available for all observations, but could be useful as additional information where available.

A decorative graphic element consisting of a teal diagonal line and a large black letter A.

Appendix

Additional information and figures are included in the Appendix. Figures and data for each area and for both wind data from Ekofisk and SAR wind will be included here.

A.1 Additional figures

The following figures have been generated as a part of this thesis, but has been included in the results and discussion section.

A.1.1 Observations

Below are additional figures that show the distribution of observations with regards to time and wind speed from Ekofisk and SAR wind.

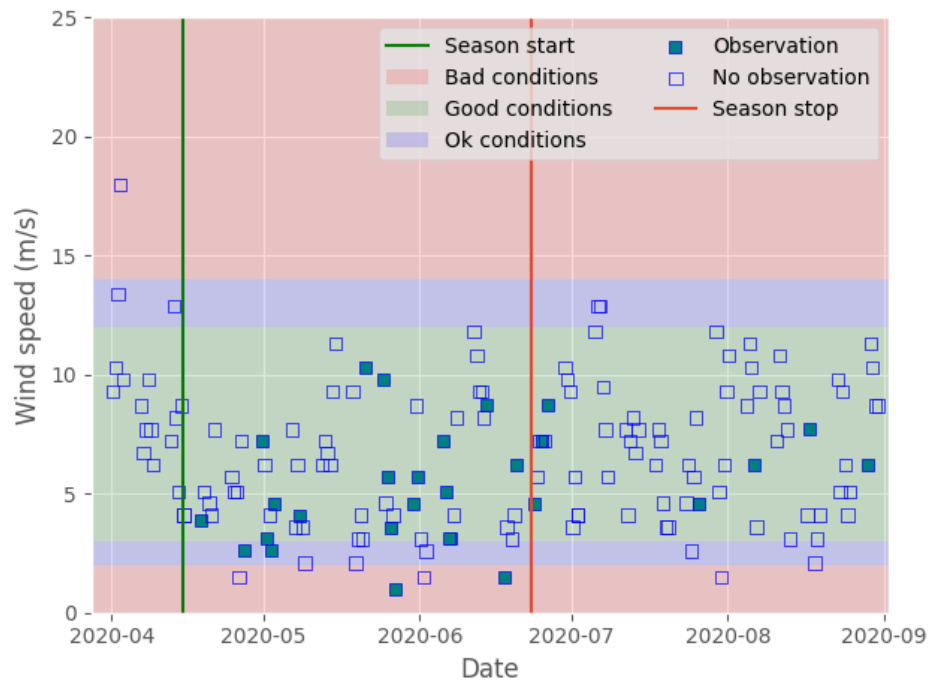


Figure A.1: Area 2 observation in 2020 with wind data from Ekofisk

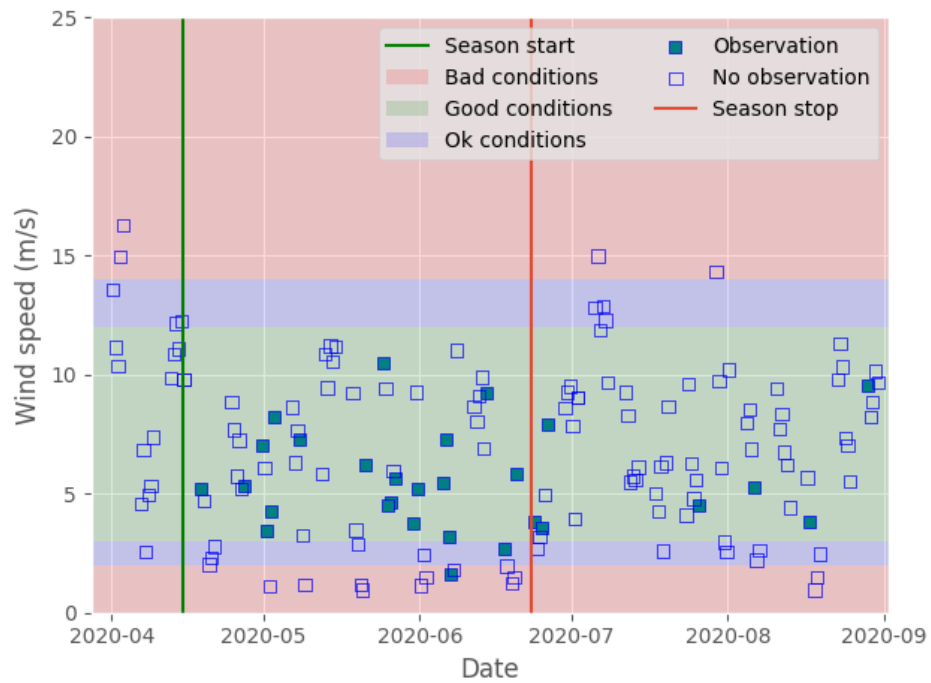


Figure A.2: Area 2 observation in 2020 with wind data from SARwind

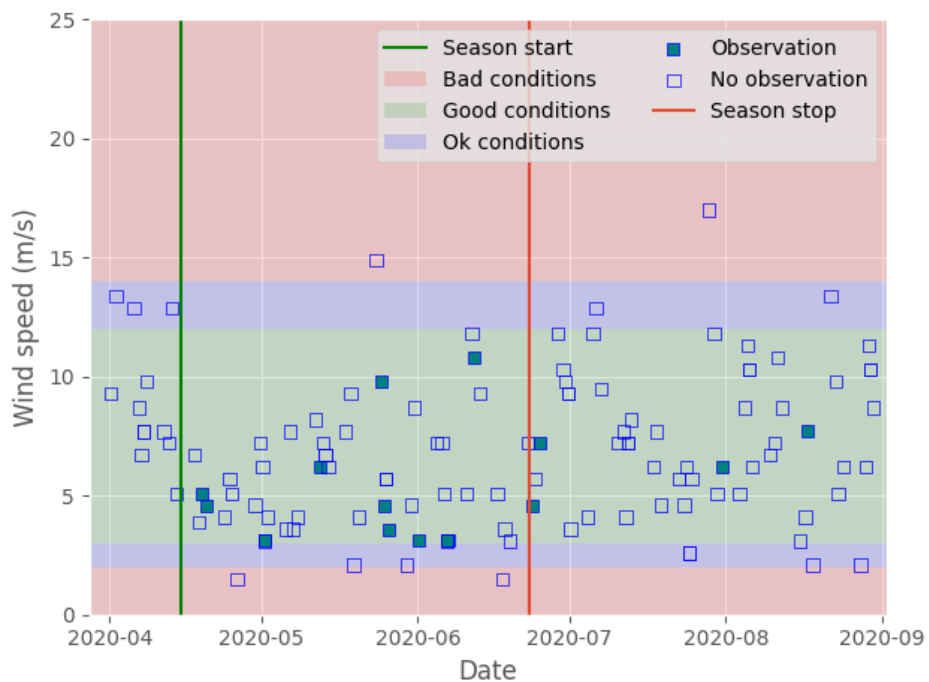


Figure A.3: Area 3 observation in 2020 with wind data from Ekofisk

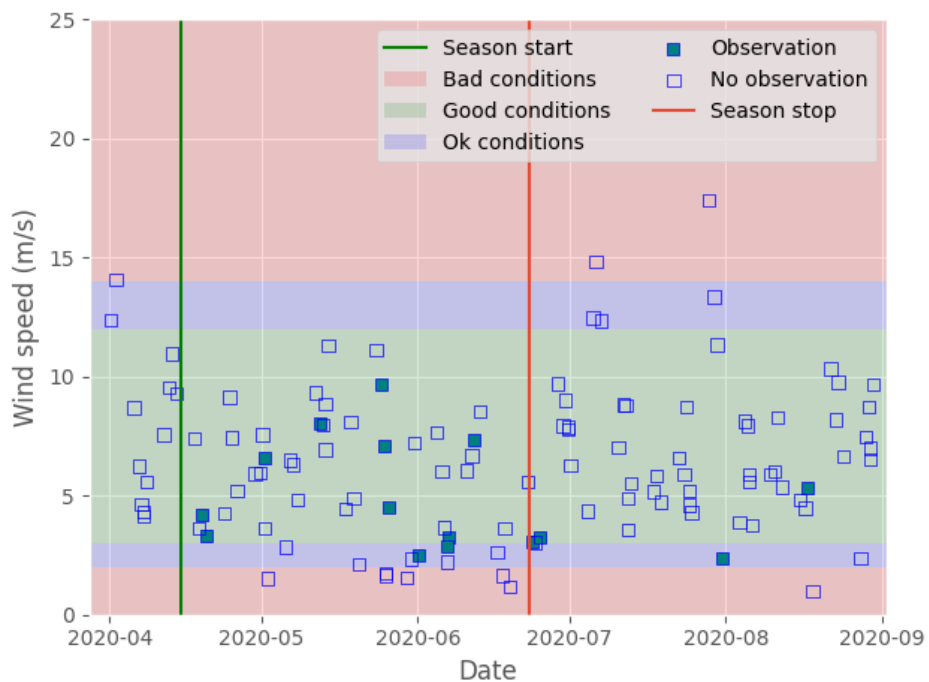


Figure A.4: Area 3 observation in 2020 with wind data from SARwind

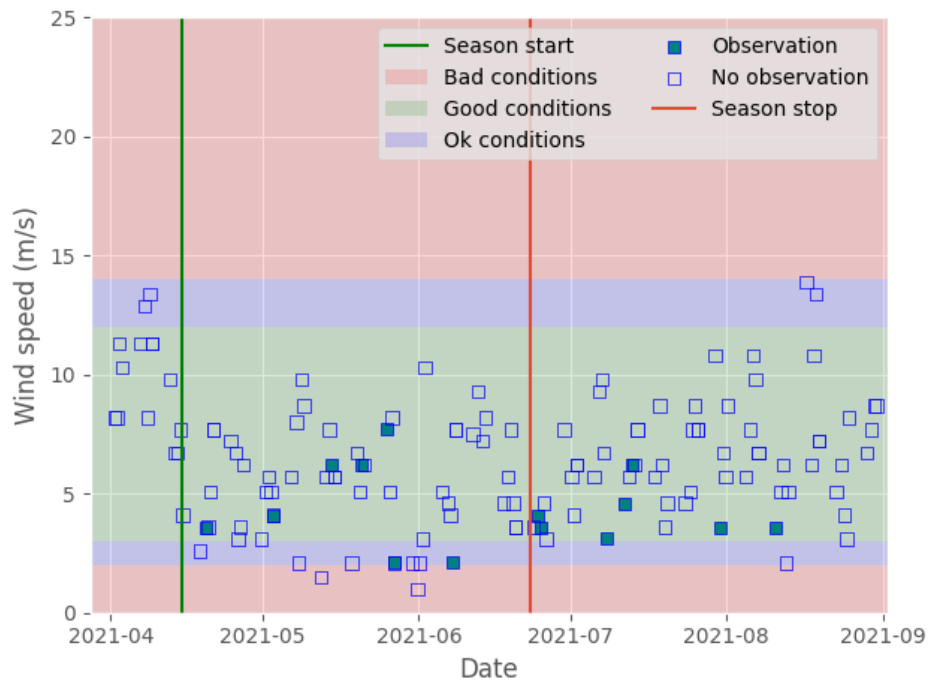


Figure A.5: Area 1 observation in 2021 with wind data from Ekofisk

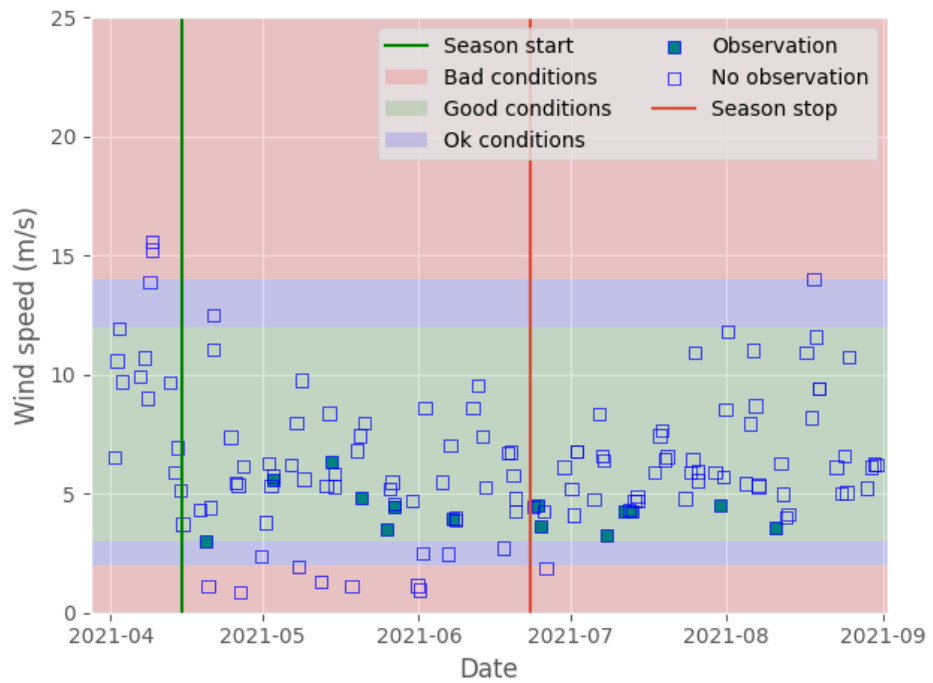


Figure A.6: Area 1 observation in 2021 with wind data from SARwind

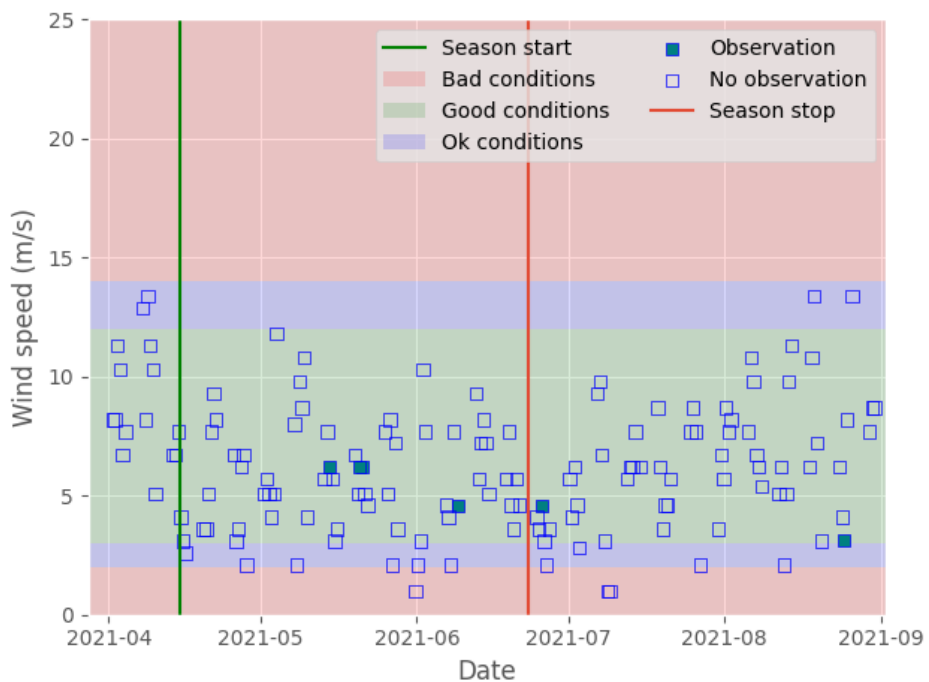


Figure A.7: Area 2 observation in 2021 with wind data from Ekofisk

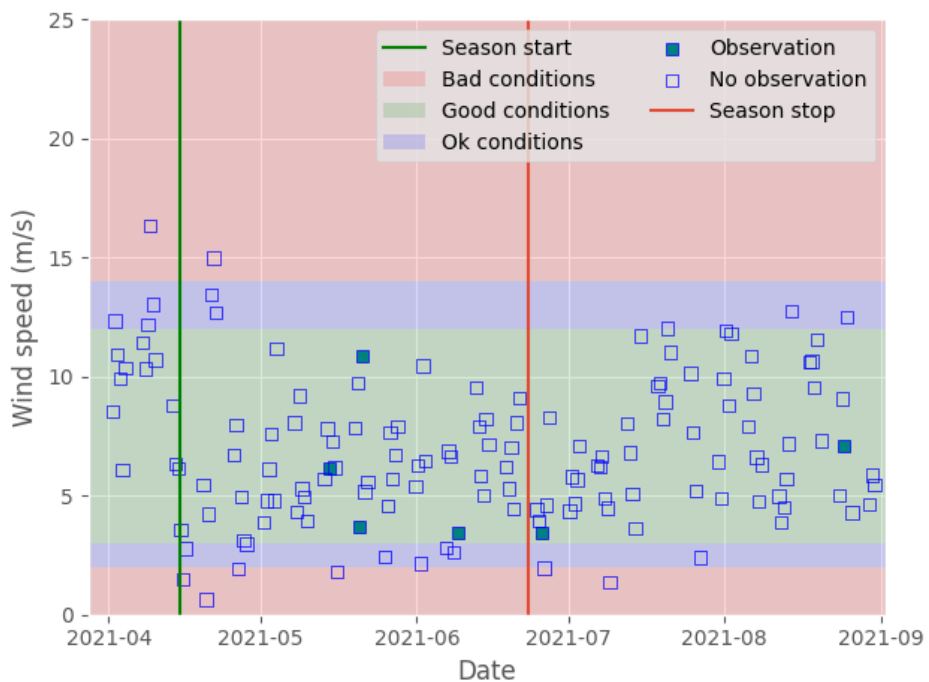


Figure A.8: Area 2 observation in 2021 with wind data from SARwind

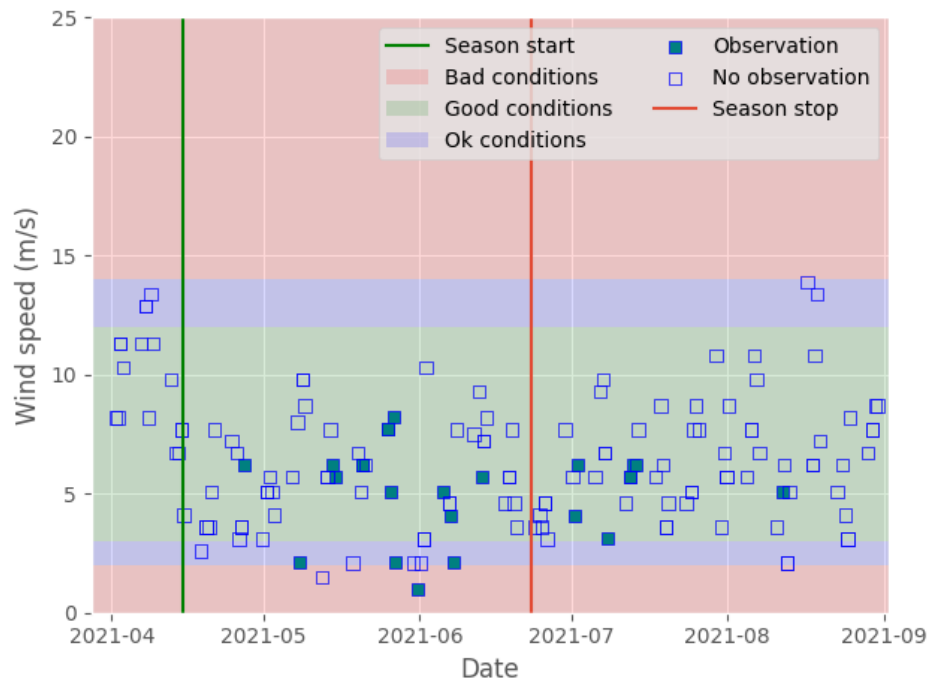


Figure A.9: Area 3 observation in 2021 with wind data from Ekofisk

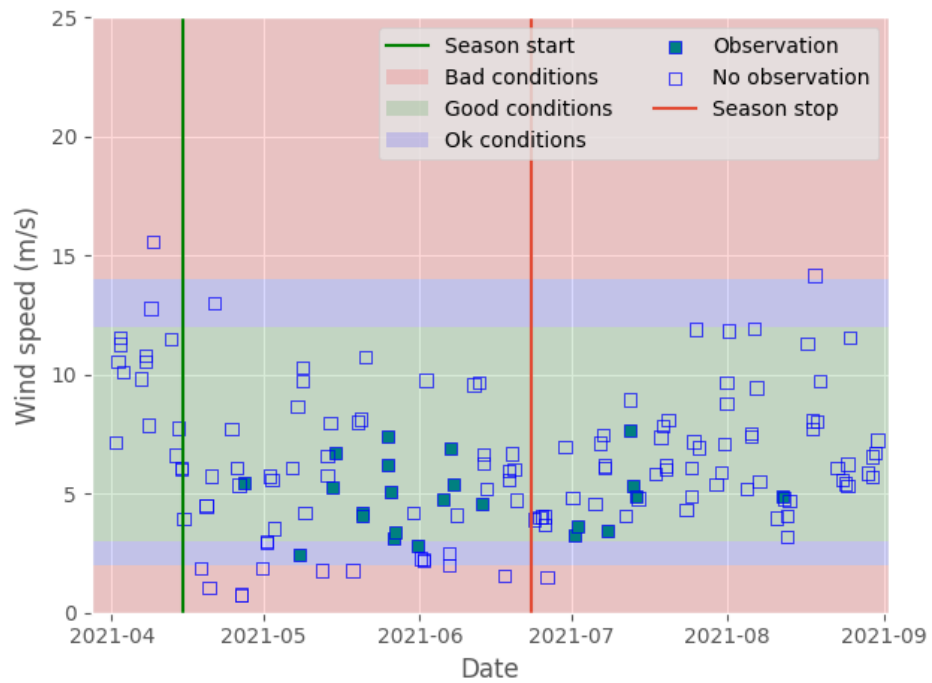


Figure A.10: Area 3 observation in 2021 with wind data from SARwind

A.1.2 Heatmaps

Below are additional figures that show the density of observations in the form of a heatmap for each area.

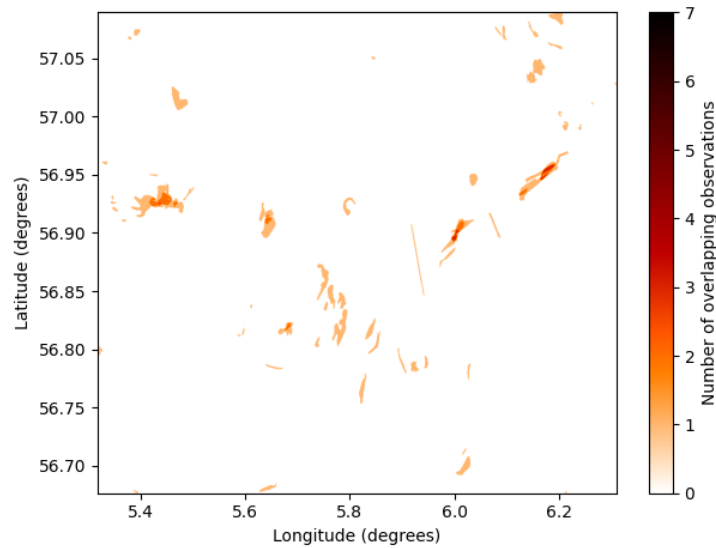


Figure A.11: Heatmap of overlapping observations for area 2 in 2020

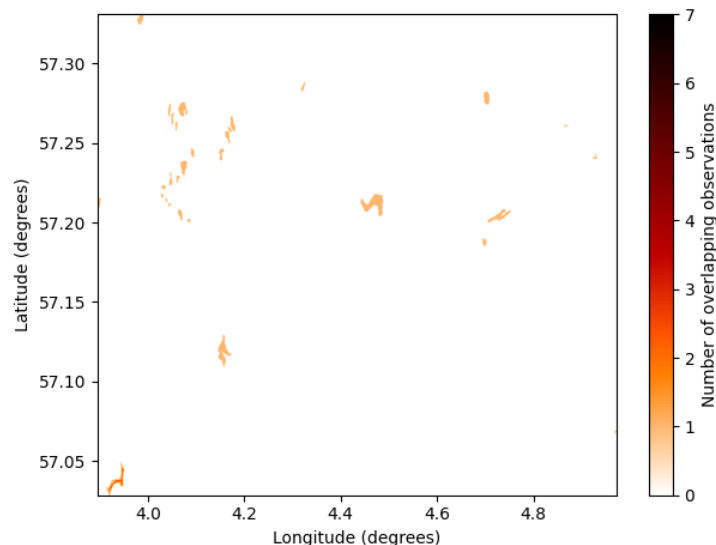


Figure A.12: Heatmap of overlapping observations for area 3 in 2020

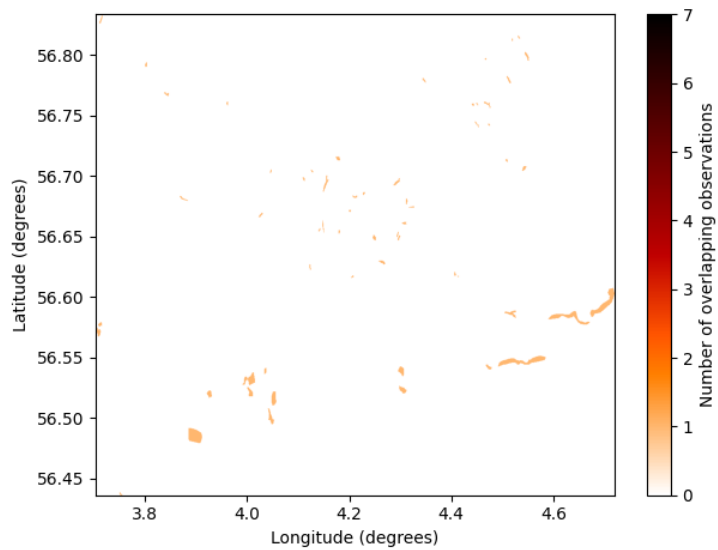


Figure A.13: Heatmap of overlapping observations for area 1 in 2021

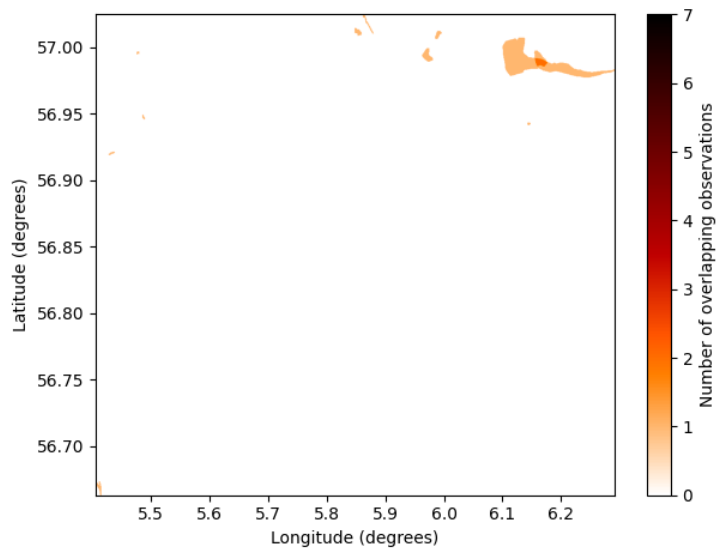


Figure A.14: Heatmap of overlapping observations for area 2 in 2021

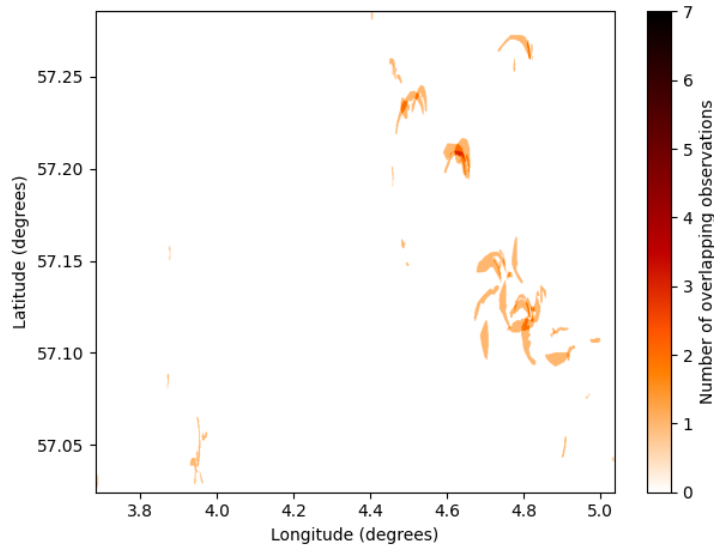


Figure A.15: Heatmap of overlapping observations for area 3 in 2021

A.1.3 Proximity plots

The remaining trawling proximity plots from 2020 and 2021 is presented here.

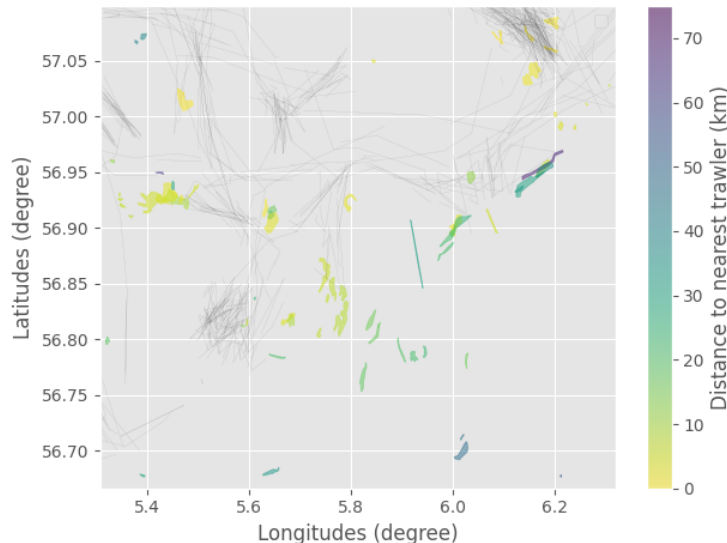


Figure A.16: Plot of all polygons colored after the distance to the closest trawler. Observations from 2020 in area 2.

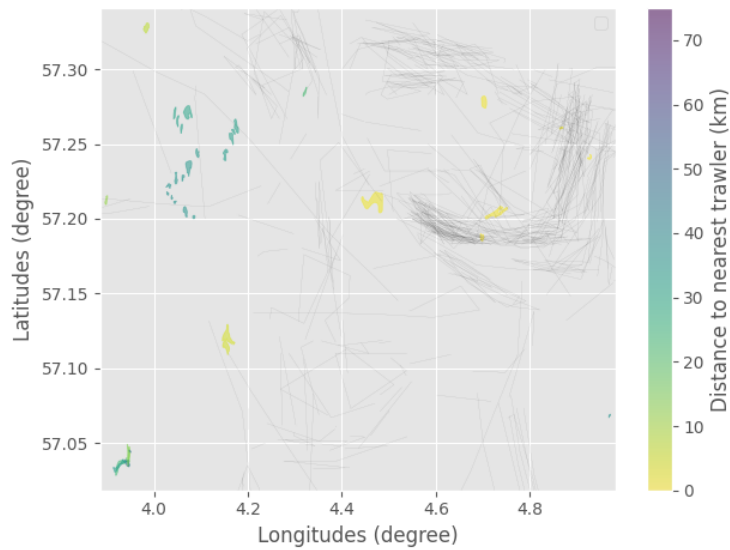


Figure A.17: Plot of all polygons colored after the distance to the closest trawler. Observations from 2020 in area 3.

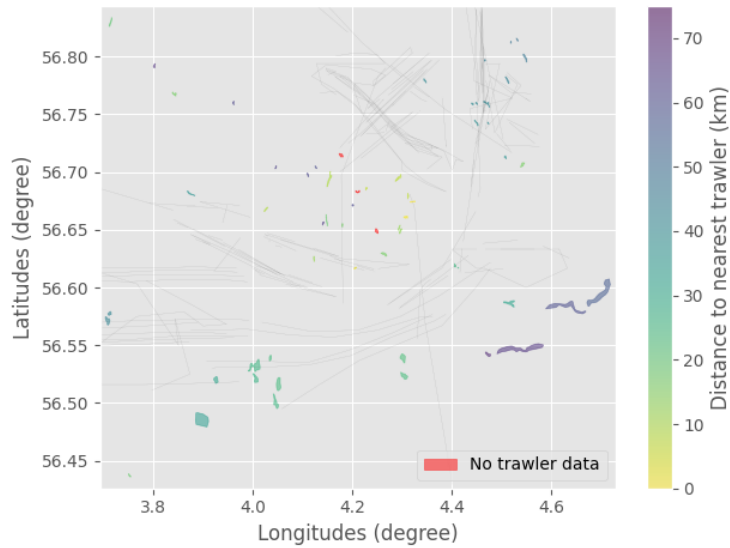


Figure A.18: Plot of all polygons colored after the distance to the closest trawler. Observations from 2021 in area 1.

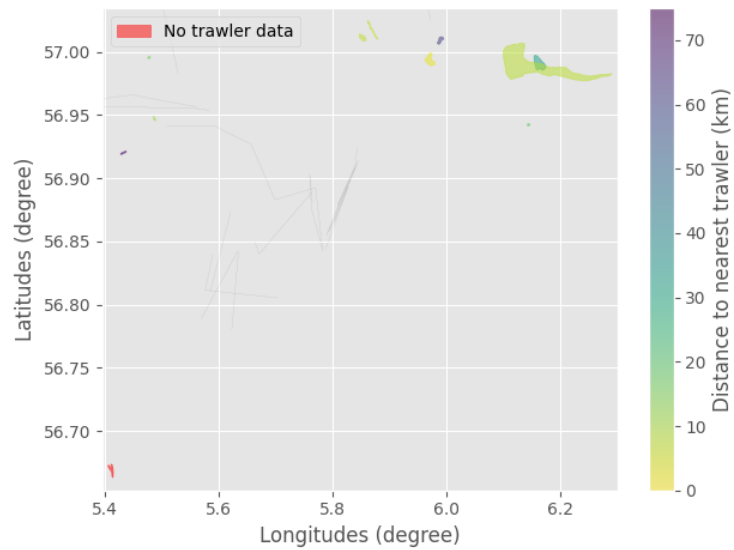


Figure A.19: Plot of all polygons colored after the distance to the closest trawler. Observations from 2021 in area 2.

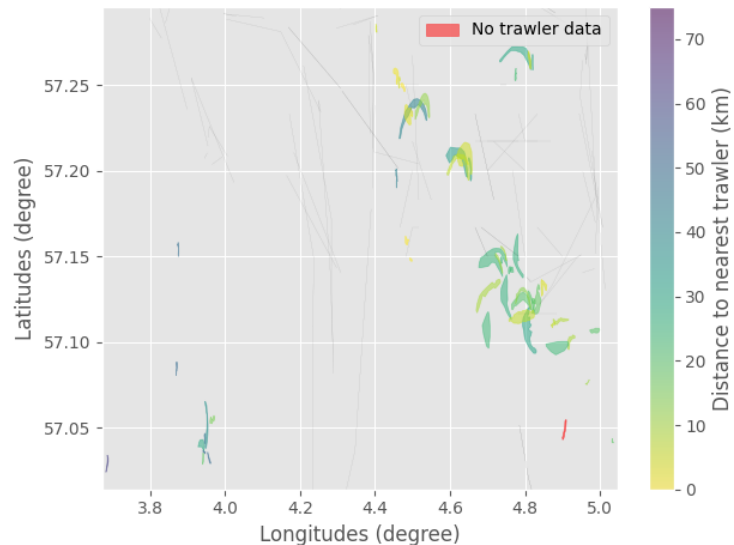


Figure A.20: Plot of all polygons colored after the distance to the closest trawler. Observations from 2021 in area 3.

Bibliography

- [1] *Bonn Agreement Oil Appearance Code*, chapter Part 3, Annex A, The Bonn Agreement Oil Appearance Code. 2016. Accessed 27.04.2023. URL: https://www.bonnagreement.org/site/assets/files/1081/special_on_volume_calculation_20160607.docx.
- [2] *Nature and Properties of Electromagnetic Waves*, chapter 2, pages 19–43. John Wiley Sons, Ltd, 2021. doi:10.1002/9781119523048.ch2.
- [3] C. Brekke and C.E. Jones. *SAR oil spill imaging, interpretation and information retrieval techniques*, pages 227–267. Radar, Sonar and Navigation. Institution of Engineering and Technology, 2020. doi:10.1049/SBRA521E_ch9.
- [4] Earthdata NASA 2023. What is synthetic aperture radar? Accessed: 02.05.2023. URL: <https://www.earthdata.nasa.gov/learn/backgrounder/what-is-sar>.
- [5] ESA 2023. Acquisition modes. Accessed: 04.05.2023. URL: <https://sentinels.copernicus.eu/web/sentinel/user-guides/sentinel-1-sar/acquisition-modes>.
- [6] ESA 2023. Orbit. Accessed: 29.05.2023. URL: <https://sentinels.copernicus.eu/web/sentinel/missions/sentinel-1/satellite-description/orbit>.
- [7] ESA 2023. Sentinel-1. Accessed: 06.02.2023. URL: https://www.esa.int/Applications/Observing_the_Earth/Copernicus/Sentinel-1.
- [8] ESA 2023. Sentinel-1 SAR Definitions. Accessed: 23.05.2023. URL: <https://sentinels.copernicus.eu/web/sentinel/user-guides/sentinel-1-sar/definitions>.
- [9] H. A. Espedal, O. M. Johannessen, J. A. Johannessen, E. Dano, D. R. Lyzenga, and J. C. Knulst. Coastwatch'95: Ers 1/2 sar detection of

- natural film on the ocean surface. *Journal of Geophysical Research: Oceans*, 103(C11):24969–24982, 1998. doi:<https://doi.org/10.1029/98JC01660>.
- [10] M. Fingas and C. E. Brown. A review of oil spill remote sensing. *Sensors*, 18(1), 2018. doi:[10.3390/s18010091](https://doi.org/10.3390/s18010091).
 - [11] Havforskningsinstituttet 2023. Tema: Tobis. Accessed: 26.05.2023. URL: <https://www.hi.no/hi/temasider/arter/tobis>.
 - [12] H. Hersbach. CMOD5.N: A C-band geophysical model function for equivalent neutral wind. *ECMWF Technical Memoranda*, (554):20, 04 2008. URL: <https://www.ecmwf.int/node/9873>, doi:[10.21957/mzcfm6jfl](https://doi.org/10.21957/mzcfm6jfl).
 - [13] J. B. Jones. Environmental impact of trawling on the seabed: A review. *New Zealand Journal of Marine and Freshwater Research*, 26(1):59–67, 1992. doi:[10.1080/00288330.1992.9516500](https://doi.org/10.1080/00288330.1992.9516500).
 - [14] Kystverket 2023. AIS Norge. Accessed: 28.04.2023. URL: <https://www.kystverket.no/navigasjonstjenester/ais/ais-artikkelside>.
 - [15] R. Lang, Y. Zhou, C. Utku, and D. Le Vine. Accurate measurements of the dielectric constant of seawater at l band. *Radio Science*, 51(1):2–24, 2016. doi:[10.1002/2015RS005776](https://doi.org/10.1002/2015RS005776).
 - [16] C. Liu, Z. Chen, Y. Shao, J. Chen, T. Hasi, and H. Pan. Research advances of sar remote sensing for agriculture applications: A review. *Journal of Integrative Agriculture*, 18(3):506–525, 2019. doi:[10.1016/S2095-3119\(18\)62016-7](https://doi.org/10.1016/S2095-3119(18)62016-7).
 - [17] B. Minchew, C. E. Jones, and B. Holt. Polarimetric analysis of backscatter from the deepwater horizon oil spill using l-band synthetic aperture radar. *IEEE Transactions on Geoscience and Remote Sensing*, 50(10):3812–3830, 2012. doi:[10.1109/TGRS.2012.2185804](https://doi.org/10.1109/TGRS.2012.2185804).
 - [18] R.K. Sharma, B.S. Kumar, N.M. Desai, and V.R. Gujraty. Sar for disaster management. *IEEE Aerospace and Electronic Systems Magazine*, 23(6):4–9, 2008. doi:[10.1109/MAES.2008.4558001](https://doi.org/10.1109/MAES.2008.4558001).
 - [19] M.I. Skolnik. *Introduction to Radar Systems*. Electrical engineering series. McGraw-Hill, 2001. URL: <https://books.google.no/books?id=Y6-APwAACAAJ>.
 - [20] A. Tripathi, V. Bhateja, and A. Sharma. Kuan modified anisotropic

diffusion approach for speckle filtering. In Jyotsna Kumar Mandal, Suresh Chandra Satapathy, Manas Kumar Sanyal, and Vikrant Bhateja, editors, *Proceedings of the First International Conference on Intelligent Computing and Communication*, pages 537–545, Singapore, 2017. Springer Singapore. doi:10.1007/978-981-10-2035-3_55.

